

# Accretion-modified Stars in Accretion Disks of Active Galactic Nuclei: Observational Characteristics in Different Regions of the Disks

JUN-RONG LIU,<sup>1,2</sup> YI-LIN WANG,<sup>1,2</sup> AND JIAN-MIN WANG<sup>1,3,4</sup>

<sup>1</sup>Key Laboratory for Particle Astrophysics, Institute of High Energy Physics, Chinese Academy of Sciences, 19B Yuquan Road, Beijing 100049, China

<sup>2</sup>School of Physics, University of Chinese Academy of Sciences, 19A Yuquan Road, Beijing 100049, China

<sup>3</sup>School of Astronomy and Space Sciences, University of Chinese Academy of Sciences, 19A Yuquan Road, Beijing 100049, China

<sup>4</sup>National Astronomical Observatory of China, 20A Datun Road, Beijing 100020, China

## ABSTRACT

Stars and compact objects embedded in accretion disks of active galactic nuclei (AGNs), dubbed as “accretion-modified star” (AMS), often experience hyper-Eddington accretion in the dense gas environment, resulting in powerful outflows as the Bondi explosion and formation of cavities. The varying gas properties across different regions of the AGN disk can give rise to diverse and intriguing phenomena. In this paper, we conduct a study on the characteristics of AMSs situated in the outer, middle, and inner regions of the AGN disk, where growth of the AMSs during the shift inwards is considered. We calculate their multiwavelength spectral energy distributions (SEDs) and thermal light curves. Our results reveal that the thermal luminosity of Bondi explosion occurring in the middle region leads to UV flares with a luminosity of  $\sim 10^{44}$  erg s<sup>-1</sup>. The synchrotron radiation of Bondi explosion in the middle and inner regions peaks at the X-ray band with luminosities of  $\sim 10^{43}$  and  $\sim 10^{42}$  erg s<sup>-1</sup>, respectively. The  $\gamma$ -ray luminosity of inverse Compton radiation spans from  $10^{42}$  to  $10^{43}$  erg s<sup>-1</sup> peaked at  $\sim 10$  MeV (outer region) and  $\sim$  GeV (middle and inner regions) bands. The observable flares of AMS in the middle region exhibits a slow rise and rapid Gaussian decay with a duration of months, while in the inner region, it exhibits a fast rise and slow Gaussian decay with a duration of several hours. These various SED and light curve features provides valuable insights into the various astronomical transient timescales associated with AGNs.

**Keywords:** Active galactic nuclei (16); Supermassive black holes (1663)

## 1. INTRODUCTION

In light of high metallicity in broad-line regions (BLRs) of active galactic nuclei (AGNs) (Hamann & Ferland 1999), stellar evolution and compact objects in AGN accretion disks were originally realized by Artymowicz et al. (1993) and Cheng & Wang (1999) for metal production in BLRs, and  $\gamma$ -ray bursts (GRBs) and gravitational waves, respectively. There is fast growing evidence for such a scenario of compact objects in the accretion disks from LIGO detections of gravitational waves (GWs). The detection of gravitational waves (GWs) from the merger of binary black holes (BBH) with masses heavier than typical stellar BHs, particularly the GW190521 event (Abbott et al. 2020), has potentially indicated that AGN disks could serve as sites for BBH mergers. Utilizing observations from the Zwicky Transient Facility (ZTF), Graham et al. (2020) reported the first potential optical electromagnetic counterpart (EMC) candidate (ZTF19abanrhr) for the GW event S190521g, which could originate from a BBH merger within an AGN disk. Although the potential association between these two astronomical transients remains a subject of ongoing debate (e.g., Ashton et al. 2021; Palmese et al. 2021; Morton et al. 2023), there is emergence of more appealing evidence from Graham et al. (2023) who subsequently reported nine EMC candidates for BBH mergers detected by LIGO/Virgo during the O3 run. Additionally, Lazzati et al. (2023), Levan et al. (2023), and Tagawa et al. (2023a) claimed several observed GRBs possibly occurring in an AGN disk. Li et al. (2023c) and Han et al. (2024) proposed that some GW events may origin from a BBH merger in AGN disks. Moreover, it would be a giant step to understand AGN phenomena of fueling the central supermassive

black holes (SMBHs) and metallicity (Wang et al. 2010, 2011, 2012, 2023b; Fan & Wu 2023) if some LIGO GW events with association with AGNs are identified eventually.

Much theoretical attention has been paid to stellar evolution, compact objects in AGN disks and related astrophysics in recent years, as summarized in Table 1. There are widespread researches on evolution of single star (Cheng & Wang 1999; Cantiello et al. 2021; Dittmann et al. 2021; McKernan et al. 2022; Jermyn et al. 2022; Ali-Dib & Lin 2023), and evolution of stellar populations via accretion in the dense environment (Wang et al. 2023b). Stars undergo supernova explosions (Grishin et al. 2021; Li et al. 2023a) in the final stage of their evolution or may even be tidally disrupted by the stellar-mass black hole (sMBH; Yang et al. 2022), leading to metal enrichment (Wang et al. 2023b; Huang et al. 2023) of the AGN disk and the formation of compact objects. The accretion onto compact objects influences their spin evolution (Jermyn et al. 2021; Chen & Lin 2023) and growth (McKernan et al. 2012; Davies & Lin 2020), giving rise to abundant observational signatures, such as Bondi explosion from powerful outflows (Wang et al. 2021a), jet flare (Wang et al. 2021b; Tagawa et al. 2023b), and the so-called “accretion-induced collapse” of neutron star (NS; Perna et al. 2021b). Numerous compact objects in the AGN disk inevitably form binary systems (Tagawa et al. 2020; Rowan et al. 2023; Wang et al. 2024) via Jacobi capture (Wang et al. 2021b), GW emission (Rom et al. 2024), dynamical friction (Qian et al. 2024), or the collision of their circum-single disks (Li et al. 2023b). Simulations of BBH evolution show that the complex interactions between the BBH and AGN disk induce the contraction of the BBH separation (Li et al. 2022; Li & Lai 2022; Dittmann et al. 2024), leading to BBH mergers (Bartos et al. 2017; Yang et al. 2019; Yi & Cheng 2019; McKernan et al. 2020; Samsing et al. 2022), often followed by electromagnetic flares (Wang et al. 2021b; Chen & Dai 2024; Tagawa et al. 2023c), such as GRB (Perna et al. 2021a; Lazzati et al. 2022; Yuan et al. 2022; Ray et al. 2023) and GRB afterglow (Wang et al. 2022). Additionally, white dwarf (WD) collisions (Luo et al. 2023; Zhang et al. 2023) and kilonova emission from NS-NS/BH-NS mergers (Zhu et al. 2021a,b; Ren et al. 2022; Kathirgamaraju et al. 2023) are also important probes for studying compact objects in AGN disks.

As the black holes in AGN disks are generally undergoing hyper-Eddington accretion ( $\sim 10^9 \dot{M}_{\text{Edd}}$ ) and dubbed as “accretion-modified stars” (AMSs; Wang et al. 2021a), where “stars” can widely refer to stars, white dwarfs, neutron stars, or black holes. In such a scenario, strong outflows develop (e.g., Wang et al. 2021a; Kitaki et al. 2021). As a consequence, outburst from the black holes emerge as the Bondi explosion through the interaction between powerful outflows and dense AGN disk gas (Wang et al. 2021a; Tagawa et al. 2022; Chen et al. 2023), resulting in thermal and non-thermal radiations (e.g., Wang et al. 2021a; Tagawa et al. 2023b). Wang et al. (2023a) first applied the AMS model to Sgr A\* with low accretion rates, naturally reproducing the orbit observed by GRAVITY/VLTI (GRAVITY Collaboration et al. 2020; Gravity Collaboration et al. 2023) and successfully explaining the period of the flare/flicking in the light curve (Genzel et al. 2003, 2010) and spectral energy distribution (SED) from radio to X-ray bands (Witzel et al. 2021; Boyce et al. 2022). It is important to note that the above AMS is situated within advection-dominated accretion flows (ADAFs; Narayan & Yi 1995; Narayan et al. 1995). Considering the environment of accretion black holes, we explore the AMSs located in the outer, middle and inner regions of the standard disk (Shakura & Sunyaev 1973), leading to distinct physical processes and observational characteristics.

This is the fourth paper in a series aimed at investigating the behavior of BHs within the AGN disks (Wang et al. 2021a,b, 2023a). This paper is structured as follows. In § 2, we present our AMS model, including the modified Bondi accretion, the formation of cavity through the interaction of strong outflows with AGN disks. § 3 provides a straightforward application of the AMS model within the context of the standard disk (inner and middle regions) and self-gravitating disk (outer region). In § 4, we calculate the thermal emissions due to free-free cooling and non-thermal radiations from the synchrotron and inverse Compton scattering processes. In § 5, we discuss the possibility of searching for astronomical transients of the Bondi explosion, especially in radio and  $\gamma$ -ray bands. Finally, in § 6, we summarize the main differences and observational signatures of the outflow and cavity in different regions of AGN disk.

## 2. THE MODEL

AMS often undergoes hyper-Eddington accretion (higher than the usual super-Eddington accretion by several orders of magnitude) in the form of Bondi accretion (e.g., Wang et al. 2021a,b). The angular momentum due to differential rotation will lead to the formation of a disk around the sMBH (see Appendix A and Figure 1) and release large amount of gravitational energy. Such a high accretion rate and energy release will give rise to outflows, which strongly impact the Bondi sphere, generating shocks and forming a cavity. The cavity is replenished under the pressure of the SMBH-disk, leading to episodic accretion onto AMS. Also, AMSs will grow heavier through accretion when migrating from the outer region of the SMBH-disk to inner region. We use the above model frame to study the outflow properties from AMSs with different mass in three regions (Section 3), including the SEDs of thermal and non-thermal emissions, light curve behaviors and its timescales determined by the accretion and outflow timescales (Section 4). We now give detailed general calculations of AMS model as follows.

**Table 1.** Studies on the stars and compact object in AGN disk.

References	star				compact object			Binary			GRB
	metallicity	accretion	evolution	SN	WD	NS	BH	formation	evolution	merger	
Cheng & Wang (1999)	✓	✓	✓					✓		✓	✓
McKernan et al. (2012)							✓				
Bartos et al. (2017)										✓	
Yang et al. (2019)										✓	
Yi & Cheng (2019)										✓	
Tagawa et al. (2020)								✓	✓		
Davies & Lin (2020)							✓				
McKernan et al. (2020)										✓	
Perna et al. (2021a)											✓
Zhu et al. (2021a)						✓					
Cantiello et al. (2021)	✓	✓									
Wang et al. (2021a)							✓				
Jermyn et al. (2021)							✓				
Perna et al. (2021b)						✓					
Dittmann et al. (2021)		✓									
Wang et al. (2021b)								✓		✓	
Zhu et al. (2021b)						✓					
Grishin et al. (2021)				✓							
Samsing et al. (2022)								✓			
Li et al. (2022)									✓		
Jermyn et al. (2022)		✓									
Yuan et al. (2022)											✓
Yang et al. (2022)			✓								
McKernan et al. (2022)			✓								
Lazzati et al. (2022)											✓
Wang et al. (2022)											✓
Li & Lai (2022)									✓		
Ren et al. (2022)						✓					
Fan & Wu (2023)	✓									✓	
Li et al. (2023b)								✓			
Tagawa et al. (2023b)							✓				
Wang et al. (2023c)										✓	
Ray et al. (2023)											✓
Chen & Lin (2023)							✓				
Li et al. (2023a)				✓							
Zhang et al. (2023)					✓						
Rowan et al. (2023)								✓			
Wang et al. (2023b)	✓	✓	✓	✓							
Luo et al. (2023)					✓						
Tagawa et al. (2023c)										✓	
Huang et al. (2023)	✓										
Kathirgamaraju et al. (2023)										✓	
Chen & Dai (2024)										✓	
Ali-Dib & Lin (2023)			✓								
Wang et al. (2023a)							✓		✓	✓	
Dittmann et al. (2024)									✓		
Qian et al. (2024)								✓			
Rom et al. (2024)								✓			
Wang et al. (2024)								✓			

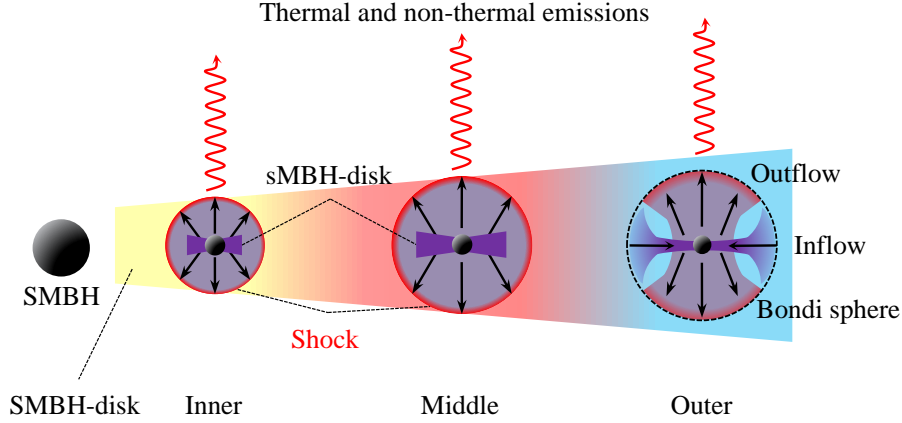


**Figure 1.** Bondi explosion of Accretion-modified Stars (AMS) embedded in AGN disk. AMSs in the inner and middle regions generate powerful outflows and form hot cavities, whereas for the AMS in the outer region, outflows and inflows coexist.

We consider AGN disks of SMBHs with mass  $M_p$  and accretion rates  $\dot{M}_p$ . It is convenient to use the dimensionless accretion rates of  $\dot{\mathcal{M}}_p = \dot{M}_p c^2 / L_{\text{Edd},p}$ , where  $L_{\text{Edd},p} = 4\pi G M_p m_p c / \sigma_T$  is the Eddington luminosity of the SMBH,  $G$  is the gravitational constant,  $m_p$  is the proton mass,  $c$  is the speed of light,  $\sigma_T$  is the Thompson scattering cross section. In this paper, we discuss the case of  $\dot{\mathcal{M}}_p \sim 1$ , namely, SMBH is accreting in the regime of Shakura-Sunyaev model (Shakura & Sunyaev 1973). We consider the simple case that the SMBH is trapped in and co-rotates with the disk, as shown in Figure 1. Then its dimensionless Bondi accretion rate is described by the Hoyle–Lyttleton–Bondi (HLB) formulation (Hoyle & Lyttleton 1939; Bondi 1952) and modified in thin disks (Kocsis et al. 2011),

$$\dot{\mathcal{M}}_s = \frac{\dot{M}_s}{\dot{M}_{\text{Edd},s}} = \frac{4\pi G^2 M_s^2 \rho_p}{(c_s^2 + \Delta v^2)^{3/2} \dot{M}_{\text{Edd},s}} \times \min \left\{ \frac{H_p}{R_{\text{Bon}}}, 1 \right\} \times \min \left\{ \frac{R_{\text{hill}}}{R_{\text{Bon}}}, 1 \right\}, \quad (1)$$

and the Bondi radius is given by

$$R_{\text{Bon}} = \frac{G M_s}{c_s^2 + \Delta v^2}, \quad (2)$$

where  $M_s$  is the mass of sMBH,  $\rho_p$  is the gas density around the sMBH,  $c_s$  is the speed of sound,  $H_p$  is the half-thickness of the SMBH-disk,  $R_{\text{hill}} = (M_s/3M_p)^{1/3} R$  is the Hill radius of the sMBH,  $R$  is the locus of the sMBH in the SMBH-disk,  $\dot{M}_{\text{Edd},s} = L_{\text{Edd},s}/c^2$ ,  $L_{\text{Edd},s} = 4\pi G M_s m_p c / \sigma_T$  is the Eddington luminosity of the sMBH,  $\Delta v = \Omega_K \times \min\{R_{\text{Bon}}, R_{\text{hill}}\}/2$  is the relative velocity between the sMBH and the gas at the Hill radius or Bondi radius,  $\Omega_K = \sqrt{G M_p / R^3}$  is the Keplerian angular velocity. The subscripts “s” and “p” refer to the secondary (i.e., sMBH) and primary black hole (i.e., SMBH) of the binary system. The second term of Equation (1) accounts for the geometry effect of the SMBH-disk, indicating that the Bondi accretion will be suppressed by a factor of  $(H_p/R_{\text{Bon}})$  if the half-thickness of the SMBH-disk is smaller than the Bondi radius  $R_{\text{Bon}}$ . The third term represents the tidal effect of the central SMBH, suggesting that only the gas located within the Hill radius will undergo accretion onto the sMBH.

Generally, Bondi accretion onto the sMBH in standard disk is hyper-Eddington due to the dense gas environment (e.g., Wang et al. 2021a), resulting in the development of powerful outflows (e.g. Ohsuga et al. 2005; Jiang et al. 2014; Wang et al. 2021a). The outflow power is

$$L_{\text{out}} = \eta_{\text{out}} \dot{M}_s c^2, \quad (3)$$

$$\eta_{\text{out}} = \eta_{\text{rad}} f_{\text{acc}} (1 - f_{\text{adv}}), \quad (4)$$

where  $\eta_{\text{out}}$  is the conversion efficiency of channeling gravitational energy into outflows,  $\eta_{\text{rad}} \approx 0.1$  denotes the radiation efficiency,  $f_{\text{adv}} \approx 0.9$  is the advection fraction, and  $f_{\text{acc}}$  is the fraction of the accretion rate onto the sMBH to the Bondi accretion rate (see Equation A2). In fact,  $f_{\text{adv}}$  is quite uncertain in consideration of advection, photon trapping and outflows (e.g., simulations in Takeuchi et al. 2009).

These powerful outflows will significantly impact the local structures of the SMBH-disk, generating a cavity (Wang et al. 2021a,b; Kimura et al. 2021) with a radius denoted as  $R_{\text{cav}}$ , provided that the kinetic energies of the outflows exceed the local dissipation rates of gravitational energy within the SMBH-disk (Wang et al. 2023a), i.e.,  $L_{\text{out}} \gtrsim 4\pi R_{\text{cav}}^3 \varepsilon_+ / 3$ , where  $\varepsilon_+ \approx Q_+ / H_p$  is the volume dissipation rates of the SMBH-disk,  $Q_+ = 3GM_p \dot{M}_p / 8\pi R^3$  is surface heating rates (Frank et al. 2002), and we here disregard the factor of the inner boundary condition of accretion disks. Based on this condition, the maximum of  $R_{\text{cav}}$  can be determined

$$R_{\text{cav}} = \left( \frac{3L_{\text{out}}}{4\pi\varepsilon_+} \right)^{1/3}. \quad (5)$$

In the outer region of the self-gravitating disks, we demonstrate that the outflows are momentum-driven since the diffusion timescale  $t_{\text{diff}}$  is much shorter than the expansion timescale  $t_{\text{out}}$ , as shown in Table 2. So the outflow velocity  $v_{\text{out}}$  and its expansion timescale  $t_{\text{out}}$  satisfy the momentum equation  $M_{\text{out}} v_{\text{out}} / t_{\text{out}} = L_{\text{out}} / c$  (King 2003) and kinematic equation  $R_{\text{out}} = v_{\text{out}} t_{\text{out}}$ , respectively, where  $R_{\text{out}} = \min\{R_{\text{Bon}}, R_{\text{hill}}, H_p, R_{\text{cav}}\}$  is the outflow radius when the mass falling from SMBH-disk is halted, and  $M_{\text{out}} = 4\pi R_{\text{out}}^3 \rho_p / 3$  is the gas mass within  $R_{\text{out}}$ . Then we obtain

$$v_{\text{out}} = \left( \frac{L_{\text{out}} R_{\text{out}}}{M_{\text{out}} c} \right)^{1/2}, \quad (6)$$

$$t_{\text{out}} = \left( \frac{M_{\text{out}} R_{\text{out}} c}{L_{\text{out}}} \right)^{1/2}. \quad (7)$$

While in the inner and middle regions, the energy-driven outflows are developed because the diffusion timescale of the photons is much longer than the expansion timescale. So the outflow velocity  $v_{\text{out}}$  and its expansion timescale  $t_{\text{out}}$  satisfy the energy equation  $L_{\text{out}} t_{\text{out}} = M_{\text{out}} v_{\text{out}}^2 / 2$ , and the kinematic equation  $R_{\text{out}} = v_{\text{out}} t_{\text{out}}$ . Then we obtain

$$v_{\text{out}} = \left( \frac{2L_{\text{out}} R_{\text{out}}}{M_{\text{out}}} \right)^{1/3}, \quad (8)$$

$$t_{\text{out}} = \left( \frac{M_{\text{out}} R_{\text{out}}^2}{2L_{\text{out}}} \right)^{1/3}. \quad (9)$$

We here approximate  $M_{\text{out}}$  as the total mass of the outflow given that the initial outflow mass from the sMBH-disk  $M_{\text{ini}} = (1 - f_{\text{acc}}) \dot{M}_s t_{\text{out}} \lesssim M_{\text{out}}$  during the time interval of  $t_{\text{out}}$  and can be ignored (see later calculations in § 3). The gravity of the gas within the Bondi radius may enhance the Bondi accretion (Wandel 1984; Kocsis et al. 2011), which depends on the ratio of  $M_{\text{out}} / M_s$ . The accretion onto the sMBH lasts for a timescale of  $t_{\text{last}} = \max\{t_{\text{out}}, t_{\text{vis}}\}$ , determined by  $t_{\text{out}}$  and the viscosity timescale of the sMBH-disk ( $t_{\text{vis}}$ , see Equation A18). Here we compare the model with the case of extremely low accretion rates (ADAF disk,  $\dot{M}_p \ll 1$ ) discussed in Wang et al. (2023a) and point out the difference that the role of external pressure of SMBH-disk are unimportant in our model. In § 3, we would demonstrate that only a small fraction of the kinetic energy is utilized to do work against the external pressure of SMBH-disk. Because the gas density in the standard disk and self-gravitating disk (see Equations 16, 27, 38, and Figure 5) is much higher than that in ADAF disk ( $\sim 10^{-14} \text{ g cm}^{-3}$ , Wang et al. 2023a) but the temperature is much lower than that in the ADAF disk ( $\sim 10^{10} \text{ K}$ , Narayan & Yi 1995), the kinematic energy of outflows is much larger than the thermal energy (i.e., the work used to overcome the external pressure) after the outflows rush out of the SMBH-disk.

If the velocity of the outflow exceeds the local sound speed, a shock will emerge and heat the gas in the SMBH-disk (e.g., Blandford & Eichler 1987). The temperature of the shocked gas can be determined using the Rankine–Hugoniot jump conditions

$$T_{\text{sh}} = \frac{2(\Gamma_{\text{ad}} - 1)m_p v_{\text{out}}^2}{(1 + \Gamma_{\text{ad}})^2 k_B}, \quad (10)$$

where the adiabatic index  $\Gamma_{\text{ad}} = 5/3$ , and  $k_B$  is the Boltzmann constant. The heated gas will quickly expand as its gas pressure increases significantly after being shocked. Once the pressure equilibrium between the shocked gas and SMBH-disk is attained,  $\rho_{\text{sh}} k_B T_{\text{sh}} / m_p = \rho_p c_s^2$ , a cavity is formed (Wang et al. 2021b). We then obtain the density of the shocked gas

$$\rho_{\text{sh}} = \frac{\rho_p c_s^2 m_p}{k_B T_{\text{sh}}}. \quad (11)$$

The hot gas in the cavity will lose its thermal energy through free-free cooling within a timescale of

$$t_{\text{cool}} = \frac{3\rho_{\text{sh}}k_{\text{B}}T_{\text{sh}}}{2m_{\text{p}}j_{\text{ff}}}, \quad (12)$$

where  $j_{\text{ff}}$  is the free-free emission coefficient.

After cooling, the cavity will be refilled under the pressure of the SMBH-disk in a rejuvenation timescale of (Wang et al. 2023a)

$$t_{\text{rej}} = \frac{R_{\text{cav}}}{v_{\text{turb}}}, \quad (13)$$

where  $v_{\text{turb}} = \alpha c_{\text{s}}$  is the turbulence velocity. After the cavity is refilled with cold gas from SMBH-disk, the above physical process will restart, indicating episodic accretion. This is very similar with the cases of seed black hole growth at high redshift (Wang et al. 2006) and accretion onto intermediate mass BHs in dense protogalactic clouds (Milosavljević et al. 2009).

Apart from the above episodic Bondi explosion, another important feature of the sMBH is the migration from the outer to inner regions due to the torque of the SMBH-disk. Here, we consider two timescales: the viscosity timescale of the SMBH-disk and the type I migration timescale given by

$$t'_{\text{vis}} = \frac{R}{v'_{\text{r}}}, \quad (14)$$

$$t_{\text{Lind}} = \frac{M_{\text{s}}R^2\Omega_{\text{K}}}{T_{\text{net}}}, \quad (15)$$

respectively, where  $v'_{\text{r}}$  is the radial velocity of the SMBH-disk,  $T_{\text{net}} = (1.364 + 0.541 \times \gamma_{\sigma})(M_{\text{s}}R\Omega_{\text{K}}/M_{\text{p}}c_{\text{s}})^2\Sigma_{\text{p}}R^4\Omega_{\text{K}}^2$  is the Lindblad torque (Tanaka et al. 2002),  $\gamma_{\sigma} = -d \ln \Sigma_{\text{p}}/d \ln R$ , and  $\Sigma_{\text{p}} = 2\rho_{\text{p}}H_{\text{p}}$  is the surface density. The real migration timescale is  $t_{\text{mig}} = \min(t'_{\text{vis}}, t_{\text{Lind}})$ .

### 3. AMS IN THE STANDARD DISK AND SELF-GRAVITATING DISK

In this paper, we employ the self-gravitating disk model in the outer region (Sirko & Goodman 2003) and standard model in the middle and inner regions (Shakura & Sunyaev 1973). The disk becomes self-gravity dominated beyond a critical radius  $R_{\text{SG}}$  determined by the Toomre parameter  $Q = \Omega_{\text{K}}c_{\text{s}}/\pi G\rho_{\text{p}}H_{\text{p}} = 1$  (Toomre 1964), which yields  $R_{\text{SG}}/R_{\text{g}} = 1.2 \times 10^3 \alpha_{0.1}^{28/45} M_{\text{g}}^{-52/45} \dot{M}_{\text{p}}^{-22/45}$  (e.g., Wang et al. 2021a).

#### 3.1. outer region

In the outer region beyond  $R_{\text{SG}} = 1.2 \times 10^3 R_{\text{g}}$ , the disk becomes self-gravitating. As described by Equations (B31), (B32), (B33), and (B35) in Appendix B, the half-thickness, gas density, sound speed of the SMBH-disk, and radial velocity are

$$\begin{cases} H_{\text{p}} = 2.3 \times 10^{16} \alpha_{0.1}^{-1/3} r_5^{3/2} \dot{M}_{\text{p}}^{1/3} M_8^{4/3} \text{ cm}, \\ \rho_{\text{p}} = 9.8 \times 10^{-15} r_5^{-3} M_8^{-2} \text{ g cm}^{-3}, \\ c_{\text{s}} = 1.5 \times 10^6 \alpha_{0.1}^{-1/3} \dot{M}_{\text{p}}^{1/3} M_8^{1/3} \text{ cm s}^{-1}, \\ v'_{\text{r}} = 3.4 \times 10^3 \alpha_{0.1}^{1/3} r_5^{1/2} \dot{M}_{\text{p}}^{2/3} M_8^{2/3} \text{ cm s}^{-1}, \end{cases} \quad (16)$$

where  $\alpha_{0.1} = \alpha/0.1$  is the viscosity parameter,  $r_5 = R/10^5 R_{\text{g}}$ , and  $M_8 = M_{\text{p}}/10^8 M_{\odot}$  denotes the mass of the central SMBH. By substituting the disk parameters into Equations (1) and (2), we can estimate the dimensionless Bondi accretion rate and Bondi radius as follows:

$$\dot{M}_{\text{s}} = 5.0 \times 10^5 \alpha_{0.1} r_5^{-3} \dot{M}_{\text{p}}^{-1} M_8^{-2} q_{\bar{6}}, \quad (17)$$

$$R_{\text{Bon}} = 6.2 \times 10^{15} \alpha_{0.1}^{2/3} \dot{M}_{\text{p}}^{-2/3} M_8^{1/3} q_{\bar{6}} \text{ cm}, \quad (18)$$

where  $q_{\bar{6}} = q/10^{-6}$ ,  $q = M_{\text{s}}/M_{\text{p}} = 10^{-6} m_2/M_8$ , and  $m_2 = M_{\text{s}}/10^2 M_{\odot}$ . First, the Bondi radius is much smaller than the disk half-thickness, so the geometry effect can be ignored. Second, the Hill radius of the sMBH is  $R_{\text{hill}} = (M_{\text{s}}/3M_{\text{p}})^{1/3} R \approx 1.0 \times 10^{16} \text{ cm}$ , much larger than the Bondi radius, so the tidal effect of the SMBH is also marginal. Third, the differential velocity  $\Delta v = \Omega_{\text{K}} R_{\text{Bon}}/2 = 2.0 \times 10^5 \text{ cm s}^{-1}$ , is about one order of magnitude lower than the sound speed, indicating that the modification to the spherical accretion can also be ignored. Finally, the sphere mass within the Bondi radius is  $M_{\text{Bon}} =$



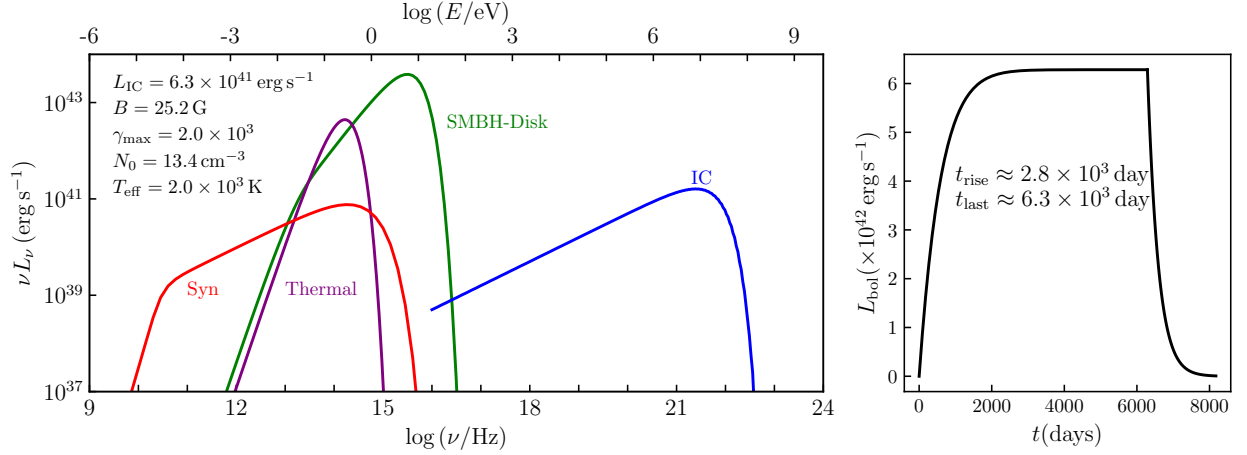


**Figure 2.** *Left:* The spectral energy distributions of the powerful outflows developed by the AMS in the outer region of the SMBH-disk and the black body radiation from the SMBH-disk. The integrated black body radiation from the SMBH-disk is shown in green. AGN disk gas is shocked by accretion powered outflows and emits thermal radiation (purple) with an effective temperature of  $T_{\text{eff}}$ . The shock formed from the strong outflows accelerates electrons in AGN disk, emitting synchrotron emissions (red) and generating high energy photons by inverse Compton scattering (blue). *Right:* The thermal light curve of the Bondi explosion, described by Equation (50), which behaves like a Heaviside step function since the inflow and outflow coexist (see Figure 1). The rise timescale and the duration are  $t_{\text{rise}} \approx t_{\text{eff}}$ ,  $t_{\text{last}} \approx t_{\text{out}}$ , respectively. The related parameters is listed in Table 2.

$4\pi R_{\text{Bon}}^3 \rho_p / 3 = 5.0 M_{\odot}$ , much smaller than the sMBH mass, implying that its gravity only has a marginal effect on enhancing the accretion process.

By replacing size  $\Delta R$  in Equation (A1) with  $R_{\text{Bon}}$ , we obtain the outer radius of the sMBH-disk as

$$X_{\text{out}} = \frac{R_{\text{Bon}}^4 M_p}{4R^3 M_s} = 1.2 \times 10^{14} \alpha_{0.1}^{8/3} r_5^{-3} \dot{M}_p^{-8/3} M_8^{-5/3} q_6^3 \text{ cm}, \quad (19)$$

corresponding to  $7.9 \times 10^6 r_g$ , where  $r_g = GM_s/c^2$  is the gravitational radius of sMBH. This gives an accretion fraction  $f_{\text{acc}} \approx 8.7 \times 10^{-4}$ . However, the formation of the sMBH-disk can be quenched by the turbulence with a size scale of  $l_{\text{turb}} \sim \alpha c_s / \Omega_K \sim \alpha H_p \sim 2.3 \times 10^{15} \text{ cm}$ , comparable with  $R_{\text{Bon}}$ . The chaotic turbulence leads to a low AM material accretion onto the sMBH (Chen & Lin 2023) and gives rise to a small size sMBH-disk as indicated by its AM expression  $\Delta \ell_s = \sqrt{X_{\text{out}} GM_s}$ . The simulations of Bondi-Hoyle accretion in a turbulent medium show that turbulence would reduce the accretion rate by a factor of a few, possibly dependent on the magnetic field and the Mach number of the accreting gas (e.g., Lee et al. 2014; Burleigh et al. 2017). In consideration of the above uncertainty of the turbulence, we set  $f_{\text{acc}} \sim 0.1$  and define a parameterized conversion efficiency  $\eta_{\text{out}}$ . With Equation (4), we obtain the conversion efficiency  $\eta_{\text{out}} \approx 10^{-3}$ . Based on Equations (3) and (17), the sMBH experiences a hyper-Eddington accretion process and forms powerful outflow with

$$L_{\text{out}} = 6.3 \times 10^{42} \eta_3 \alpha_{0.1} r_5^{-3} \dot{M}_p^{-1} M_8^{-1} q_6^2 \text{ erg s}^{-1}, \quad (20)$$

where  $\eta_3 = \eta_{\text{out}} / 10^{-3}$ .

With the condition that the power of the outflow exceeds the local heat production rate of the AGN disk, the cavity radius is given by Equations (5) and (20) as  $R_{\text{cav}} = 1.7 \times 10^{18} \text{ cm}$ , much larger than the disk half-thickness. This indicates that the outflow can rush out of the disk and significantly change the local disk structure. In this case, the maximum of cavity radius is

$$R_{\text{cav}} = H_p = 2.3 \times 10^{16} \alpha_{0.1}^{-1/3} r_5^{3/2} \dot{M}_p^{1/3} M_8^{4/3} \text{ cm}. \quad (21)$$

The gas mass within the cavity is given by  $M_{\text{cav}} = 4\pi R_{\text{cav}}^3 \rho_p / 3 = 2.4 \times 10^2 M_{\odot}$ . When the accretion is halted, the outflow radius is  $R_{\text{out}} = \min\{R_{\text{Bon}}, R_{\text{hill}}, H_p, R_{\text{cav}}\} = R_{\text{Bon}} = 6.2 \times 10^{15} \text{ cm}$  and the outflow mass is  $M_{\text{out}} = 4\pi R_{\text{out}}^3 \rho_p / 3 = 5.0 M_{\odot}$ . Based on Equations (6), (7), and (20), we derive the velocity of the outflow and its expansion timescale as

$$v_{\text{out}} = 1.2 \times 10^7 \eta_3^{1/2} \alpha_{0.1}^{-1/6} \dot{M}_p^{1/6} M_8^{1/6} \text{ cm s}^{-1}, \quad (22)$$

$$t_{\text{out}} = 17.2 \eta_3^{-1/2} \alpha_{0.1}^{5/6} \dot{M}_p^{-5/6} M_8^{1/6} q_6 \text{ yr}. \quad (23)$$

The energy of outflows is  $E_{\text{out}} = L_{\text{out}} t_{\text{out}} = 3.4 \times 10^{51}$  erg. We calculate the energy required to do work against the external pressure and the AMS gravity. First, the energy used to overcome the pressure of the SMBH-disk is  $E_p = 4\pi P R_{\text{out}}^3/3 = 1.0 \times 10^{48}$  erg, much smaller than  $E_{\text{out}}$ , indicating that it is easy to overcome the disk pressure and the effect can be ignored. Second, the energy used to overcome the gravity of the AMS is  $E_g = G(M_{\text{out}} + M_s)M_{\text{out}}/R_{\text{out}} = 2.2 \times 10^{46}$  erg. These two considerations verify that almost all of the dissipated energy of the sMBH-disk is transformed into the kinetic energy of the outflow  $E_{\text{out}}$ . We also calculate the initial mass of outflows  $M_{\text{ini}} \approx (1 - f_{\text{acc}})\dot{M}_s t_{\text{out}} = 1.7 M_{\odot} \lesssim M_{\text{out}}$ , validating the previous approximation of ignoring it in Equations (22) and (23).

The velocity of the outflow is about one order of magnitude larger than the sound speed, inevitably leading to shock formation and the generation of relativistic electrons and non-thermal radiation, as shown in Figure 2. In the meanwhile, based on Equations (10) and (22), the gas will be heated to a high temperature  $T_{\text{sh}} = 3.0 \times 10^5$  K by the strong shock. Utilizing the pressure equilibrium condition between the shocked gas and SMBH-disk in Equation (11), we derive the density of shocked gas  $\rho_{\text{sh}} = 8.5 \times 10^{-16} \text{ cm}^{-3}$ , much lower than the density of the SMBH-disk gas. After the outflow rushes out of the SMBH-disk, it will form a cavity of shocked gas with high temperature and low density. The hot gas would lose its thermal energy mainly by free-free cooling with a cooling timescale of  $t_{\text{cool}} = 2.2$  d given by Equation (12), much shorter than the cavity expansion timescale  $t_{\text{out}}$ .

After the hot gas in the cavity is cooled quickly by free-free emission, the cavity would be refilled with the surrounding cold gas turbulence. Based on Equations (13) and (21), the cavity can be refilled in a rejuvenation timescale of

$$t_{\text{rej}} = 4.9 \times 10^3 \alpha_{0.1}^{-1} r_5^{3/2} M_8 \text{ yr}. \quad (24)$$

The rejuvenation is much slower than the cavity formation and leads to episodic accretion. Although the sMBH-disk size is much smaller than the result of Equation (19), we calculate the lower limit of the radial velocity of the sMBH-disk and the upper limit of the viscosity timescale based on Equations (A17), (A18), and (19),

$$v_r = 4.3 \times 10^5 \alpha_{0.1}^{-1/3} r_5^{3/2} \dot{M}_p^{4/3} M_8^{-4/3} q_6^{-1} \text{ cm s}^{-1}, \quad (25)$$

$$t_{\text{vis}} = 8.7 \alpha_{0.1}^3 r_5^{-9/2} \dot{M}_p^{-4} M_8^{-3} q_6^4 \text{ yr}, \quad (26)$$

which is smaller than the expansion timescale  $t_{\text{out}}$ . This means that the inflow and outflow coexist, as shown in Figure 1. The sMBH-disk gas will keep accreting onto the sMBH for a timescale of  $t_{\text{last}} = \max\{t_{\text{out}}, t_{\text{vis}}\} = t_{\text{out}}$ , until the outflow expands to the Bondi radius. The corresponding duty cycle is  $\delta = t_{\text{last}}/(t_{\text{last}} + t_{\text{rej}}) = 3.5 \times 10^{-3}$ . The average mass growing timescale of the sMBH is  $t_{\text{grow}} = M_s/f_{\text{acc}}\delta\dot{M}_s\dot{M}_{\text{Edd},s} = 2.6 \times 10^6 \text{ yr}$ . Using Equations (14) and (15), we obtain the viscosity timescale of the SMBH-disk  $t'_{\text{vis}} = 1.4 \times 10^7 \text{ yr}$ , and type I migration timescale  $t_{\text{Lind}} = 1.1 \times 10^7 \text{ yr}$ , respectively, where  $\gamma_{\sigma} = -d \ln \Sigma_p / d \ln R = 3/2$  is used. The real migration timescale of the sMBH is  $t_{\text{mig}} = t_{\text{Lind}}$ . For an exponentially growing case, the sMBH mass can grow up to  $M'_s = \exp(t_{\text{Lind}}/t_{\text{grow}})M_s = 69.0 M_s$ .

### 3.2. middle region

In the middle region of the standard disk, gas pressure prevails over radiation pressure, and the electron scattering optical depth is significantly larger than the absorption. According to the standard model, the radius of the middle region is  $3.0 \times 10^2 (\alpha_{0.1} M_8)^{2/21} \dot{M}_p^{16/21} < R/R_g \leq 5.1 \times 10^3 \dot{M}_p^{2/3}$  (Svensson & Zdziarski 1994), and the half-thickness, density, midplane temperature, sound speed, and radial velocity of the SMBH-disk are (Kato et al. 2008)

$$\begin{cases} H_p = 3.6 \times 10^{13} \alpha_{0.1}^{-1/10} r_3^{21/20} \dot{M}_p^{1/5} M_8^{9/10} \text{ cm}, \\ \rho_p = 3.4 \times 10^{-9} \alpha_{0.1}^{-7/10} r_3^{-33/20} \dot{M}_p^{2/5} M_8^{-7/10} \text{ g cm}^{-3}, \\ T_c = 3.2 \times 10^4 \alpha_{0.1}^{-1/5} r_3^{-9/10} \dot{M}_p^{2/5} M_8^{-1/5} \text{ K}, \\ c_s = 2.3 \times 10^6 \alpha_{0.1}^{-1/10} r_3^{-9/20} \dot{M}_p^{1/5} M_8^{-1/10} \text{ cm s}^{-1}, \\ v'_r = 5.9 \times 10^2 \alpha_{0.1}^{4/5} r_3^{-2/5} \dot{M}_p^{2/5} M_8^{-1/5} \text{ cm s}^{-1}, \end{cases} \quad (27)$$

where  $r_3 = R/10^3 R_g$ .

As discussed in § 3.1, the sMBH grows heavier due to the episodic accretion during the migration. We therefore consider a sMBH with  $10^3 M_{\odot}$  mass in the middle region. By substituting the disk parameters into Equations (1) and (2), we can estimate the dimensionless modified Bondi accretion rate and Bondi radius as follows:

$$\dot{M}_s = 1.7 \times 10^7 \alpha_{0.1}^{-4/5} r_3^{-1/10} \dot{M}_p^{3/5} M_8^{1/5} q_5^{-1/3}, \quad (28)$$



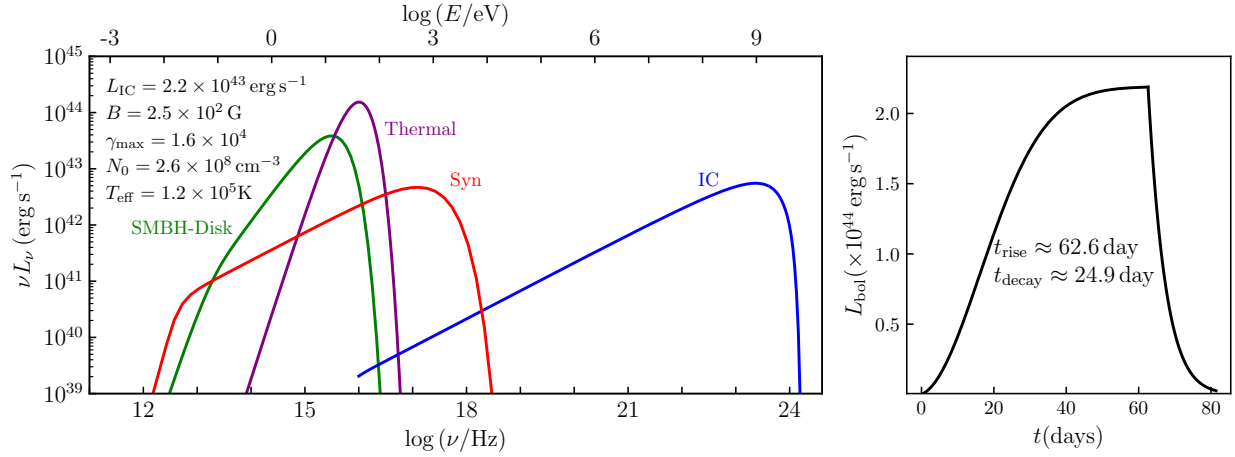


**Figure 3.** The same as the Figure 2 but for the middle region in the SMBH-disk. *Left:* The black body radiation of the SMBH-disk is shown in green. The shocked SMBH-disk gas emits thermal radiation (purple) with an effective temperature of  $T_{\text{eff}}$ . Non-thermal electrons accelerated through shocks emit synchrotron emissions (red) and generating high energy photons by inverse Compton scattering (blue). *Right:* The thermal light curve experiences slow rise and rapid decay with timescales of  $t_{\text{rise}} \approx t_{\text{last}}$  and  $t_{\text{decay}} \approx t_{\text{eff}}$ , respectively.

$$R_{\text{Bon}} = 2.7 \times 10^{15} r_3 M_8 q_5^{1/3} \text{ cm}, \quad (29)$$

where  $q_5 = q/10^{-5}$ ,  $q = M_s/M_p = 10^{-5} m_3/M_8$ , and  $m_3 = M_s/10^3 M_\odot$ . First, the Bondi radius is significantly larger than the SMBH-disk half-thickness, leading to a suppression of the Bondi accretion rate by about two orders of magnitude. Second, the Hill radius, given by  $R_{\text{hill}} = (M_s/3M_p)^{1/3} R \approx 2.2 \times 10^{14} \text{ cm}$ , is also smaller than the Bondi radius, resulting in a suppression of the Bondi accretion rate by one order of magnitude. Third, we calculate the differential velocity  $\Delta v = \Omega_K R_{\text{hill}}/2 = 7.1 \times 10^6 \text{ cm s}^{-1}$ , which is approximately three times larger than the sound speed. This suggests that the accretion deviates from spherical Bondi accretion. So we here ignore the sound speed when calculating  $\dot{\mathcal{M}}_s$  and  $R_{\text{Bon}}$ . Finally, the gas mass within the Hill radius is  $M_{\text{Bon}} = 2\pi H_p R_{\text{hill}}^2 \rho_p/3 = 6.4 M_\odot$ , much smaller than the SMBH mass, indicating that the enhancement effect on the accretion rate from the gas self-gravity within the Bondi sphere is marginal.

By substituting  $\Delta R$  in Equation (A1) with  $R_{\text{hill}}$ , we can determine the outer radius of the SMBH-disk as

$$X_{\text{out}} = \frac{R_{\text{hill}}^4 M_p}{4R^3 M_s} = 1.8 \times 10^{13} r_3 M_8 q_5^{1/3} \text{ cm}. \quad (30)$$

This corresponds to  $1.2 \times 10^5 r_g$ , resulting in an accretion fraction of  $f_{\text{acc}} \approx 6.9 \times 10^{-3}$ . Utilizing Equation (4), we derive a conversion efficiency of  $\eta_{\text{out}} \approx 6.9 \times 10^{-5}$ . Here we would like to point out that the turbulence scale  $l_{\text{turb}} \sim \alpha H_p \sim 0.1 H_p$  is much smaller than the size of accretion region  $\min\{R_{\text{Bon}}, R_{\text{hill}}, H_p\} = H_p$ , so the turbulence would not affect the formation of SMBH-disk and can be ignored. Based on Equation (3) and (28), the SMBH forms outflows with a power given by

$$L_{\text{out}} = 2.2 \times 10^{44} \eta_4 \alpha_{0.1}^{-4/5} r_3^{-1/10} \dot{\mathcal{M}}_p^{3/5} M_8^{6/5} q_5^{2/3} \text{ erg s}^{-1}, \quad (31)$$

where  $\eta_4 = \eta_{\text{out}}/10^{-4}$ .

Based on Equations (5) and (31), the powerful outflows interact with the SMBH-disk and form a cavity with a radius of  $R_{\text{cav}} = 6.5 \times 10^{15} \text{ cm}$ , which is much larger than the half-thickness of the SMBH-disk. This indicates that the outflow can rapidly rush out of the SMBH-disk and significantly alter its local structure. Therefore, the maximum of cavity radius is

$$R_{\text{cav}} = H_p = 3.6 \times 10^{13} \alpha_{0.1}^{-1/10} r_3^{21/20} \dot{\mathcal{M}}_p^{1/5} M_8^{9/10} \text{ cm}. \quad (32)$$

The gas mass within the cavity is  $M_{\text{cav}} = 4\pi R_{\text{cav}}^3 \rho_p/3 = 0.34 M_\odot$ . When the accretion is halted, the outflow radius is  $R_{\text{out}} = \min\{R_{\text{Bon}}, R_{\text{hill}}, H_p, R_{\text{cav}}\} = H_p = 3.6 \times 10^{13} \text{ cm}$  and the outflow mass is  $M_{\text{out}} = 4\pi R_{\text{out}}^3 \rho_p/3 = 0.34 M_\odot$ . With Equations (8), (9), and (31), the velocity of the outflow and its expansion timescale are derived as,

$$v_{\text{out}} = 2.9 \times 10^8 \eta_4^{1/3} \alpha_{0.1}^{1/30} r_3^{-11/60} \dot{\mathcal{M}}_p^{-1/15} M_8^{1/30} q_5^{2/9} \text{ cm s}^{-1}, \quad (33)$$

$$t_{\text{out}} = 1.5 \eta_4^{-1/3} \alpha_{0.1}^{-2/15} r_3^{37/30} \dot{\mathcal{M}}_p^{4/15} M_8^{13/15} q_5^{-2/9} \text{ d}. \quad (34)$$

The energy of outflows is  $E_{\text{out}} = L_{\text{out}} t_{\text{out}} = 2.8 \times 10^{49} \text{ erg}$ . We calculate the energy required to do work against the external pressure and the AMS gravity. First, the energy used to overcome the pressure of the SMBH-disk is  $E_p = 4\pi P R_{\text{out}}^3/3 = 3.7 \times 10^{45} \text{ erg}$ . Second, the energy used to overcome the gravity of the AMS is  $E_g = G M_{\text{out}} M_s / R_{\text{out}} = 2.5 \times 10^{48} \text{ erg}$ . These two kinds of energies are much smaller than the outflow energy  $E_{\text{out}}$ , indicating that the influence of SMBH-disk pressure and AMS gravity on the outflow expansion could be ignored. We also calculate the initial mass of outflows  $M_{\text{ini}} \approx (1 - f_{\text{acc}}) \dot{M}_s t_{\text{out}} = 0.15 M_{\odot} \lesssim M_{\text{out}}$ , which verifies the validity of the former approximation of ignoring it in Equations (33) and (34).

The outflow velocity is about two orders of magnitude larger than the local sound speed, which would give rise to powerful shocks when the outflows collide with the SMBH-disk gas. The shocks would accelerate the electrons and lead to non-thermal emissions, as can be seen in Figure 3. In the meanwhile, the shock will heat the SMBH-disk gas to an extremely high temperature  $T_{\text{sh}} = 1.9 \times 10^8 \text{ K}$  given by Equation (10) and (33). Utilizing the pressure equilibrium condition between the shocked gas and SMBH-disk based on Equation (11), we derive the density of the shocked gas  $\rho_{\text{sh}} = 1.2 \times 10^{-12} \text{ g cm}^{-3}$ , about three orders of magnitude lower than the density of the SMBH-disk gas. With Equation (12), the cooling timescale of the shocked gas is given by  $t_{\text{cool}} = 3.4 \times 10^3 \text{ s}$ , much shorter than the cavity expansion timescale, indicating that the free-free cooling mechanism is very efficient.

After the hot gas in the cavity is rapidly cooled, the cavity, based on Equations (13) and (32), will be refilled in a rejuvenation timescale of

$$t_{\text{rej}} = 4.9 \alpha_{0.1}^{-1} r_3^{3/2} M_8 \text{ yr}. \quad (35)$$

This rejuvenation is much slower than the cavity expansion. Based on Equations (A17), (A18), and (30), we can derive the radial velocity and the viscosity timescale of the sMBH-disk,

$$v_r = 3.4 \times 10^6 \alpha_{0.1} r_3^{-1/2} q_5^{1/3} \text{ cm s}^{-1}, \quad (36)$$

$$t_{\text{vis}} = 62.6 \alpha_{0.1}^{-1} r_3^{3/2} M_8 \text{ d}, \quad (37)$$

The viscosity timescale is much longer than the expansion timescale  $t_{\text{out}}$ . This means that after the outflows rush out of the SMBH-disk, the accretion onto AMS still continues and lasts for a timescale of  $t_{\text{last}} = \max\{t_{\text{out}}, t_{\text{vis}}\} = t_{\text{vis}}$ . The duty cycle of the accretion process is  $\delta = t_{\text{last}} / (t_{\text{last}} + t_{\text{rej}}) = 3.4 \times 10^{-2}$ . The average net mass accretion rate of the sMBH is  $\dot{M}_{\text{ave}} = f_{\text{acc}} \delta \dot{\mathcal{M}}_s \dot{M}_{\text{Edd},s} = 4.2 \times 10^3 \dot{M}_{\text{Edd},s}$ . The average mass growing timescale of the sMBH is  $t_{\text{grow}} = M_s / \dot{M}_{\text{ave}} = 1.1 \times 10^5 \text{ yr}$ . Using Equations (14) and (15), we obtain the viscosity timescale of the SMBH-disk,  $t'_{\text{vis}} = 7.9 \times 10^5 \text{ yr}$ , and type I migration timescale,  $t_{\text{Lind}} = 6.4 \times 10^2 \text{ yr}$ , respectively, where  $\gamma_{\sigma} = -d \ln \Sigma_p / d \ln R = 3/5$  is used. The real migration timescale of the sMBH is  $t_{\text{mig}} = t_{\text{Lind}} \ll t_{\text{grow}}$ , indicating that the sMBH can hardly grow up before migrating to the inner region.

### 3.3. inner region

In the inner region of a standard disk, radiation pressure prevails over gas pressure, and the electron scattering depth is significantly greater than absorption. According to the standard model, the inner region radius is  $R/R_g \leq 3.0 \times 10^2 (\alpha_{0.1} M_8)^{2/21} \dot{\mathcal{M}}_p^{16/21}$  (Equation 13 or 25 in Svensson & Zdziarski 1994), and the half-thickness, density, midplane temperature, sound speed, and radial velocity of the SMBH-disk are (Kato et al. 2008)

$$\begin{cases} H_p &= 1.2 \times 10^{12} M_8 \dot{\mathcal{M}}_p \text{ cm}, \\ \rho_p &= 2.0 \times 10^{-8} \alpha_{0.1}^{-1} M_8^{-1} \dot{\mathcal{M}}_p^{-2} r_1^{3/2} \text{ g cm}^{-3}, \\ T_c &= 4.8 \times 10^5 \alpha_{0.1}^{-1/4} M_8^{-1/4} r_1^{-3/8} \text{ K}, \\ c_s &= 8.0 \times 10^7 \dot{\mathcal{M}}_p r_1^{-3/2} \text{ cm s}^{-1}, \\ v'_r &= 3.1 \times 10^5 \alpha_{0.1} \dot{\mathcal{M}}_p^2 r_1^{-5/2} \text{ cm s}^{-1}, \end{cases} \quad (38)$$

where  $r_1 = R/10 R_g$  is the radius of the disk from the SMBH.

As discussed in § 3.2, the sMBH hardly grows up due to its quick migration. We therefore still consider an sMBH with  $10^3 M_{\odot}$  mass in the inner region. Substituting the disk parameters into Equations (1) and (2), the Bondi accretion rate and Bondi radius can be estimated,

$$\dot{\mathcal{M}}_s = 3.9 \times 10^5 \alpha_{0.1}^{-1} r_1 q_5^{-2/3}, \quad (39)$$

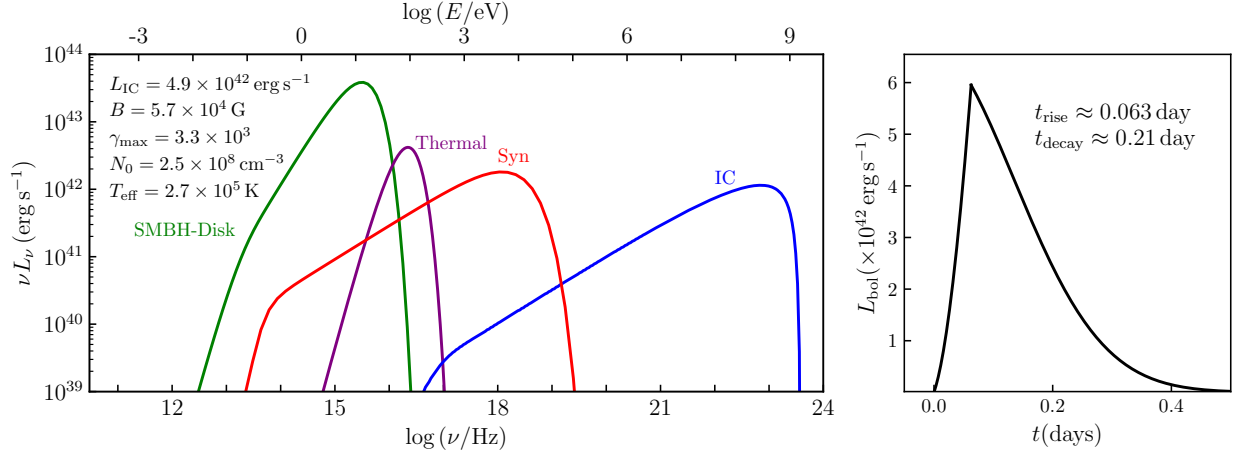


**Figure 4.** The same as the Figure 3 but for the outer region in the SMBH-disk. *Left:* The black body radiation of the SMBH-disk is shown in green. The shocked SMBH-disk gas emits thermal radiation (purple) with an effective temperature of  $T_{\text{eff}}$ . Non-thermal electrons accelerated through shocks emit synchrotron emissions (red) and generating high energy photons by inverse Compton scattering (blue). *Right:* The thermal light curve increases rapidly within a timescale of  $t_{\text{rise}} \approx t_{\text{last}}$  and decreases in a timescale of  $t_{\text{decay}} \approx t_{\text{eff}}$ , in contrast to the middle region case.

$$R_{\text{Bon}} = 2.1 \times 10^{13} M_8 \dot{M}_p^{-2} r_1^3 q_5 \text{ cm}. \quad (40)$$

To derive Equations (39) and (40), four conditions are considered. First, the Hill radius  $R_{\text{hill}} = (M_s/3M_p)^{1/3} R \approx 2.2 \times 10^{12} \text{ cm}$ , which is about one order of magnitude smaller than the Bondi radius. This indicates that the tidal effect of SMBH must be considered. Second, the Bondi radius is about one order of magnitude larger than the SMBH-disk half-thickness, which means that the SMBH-disk geometry would suppress the accretion rate. Third, the differential velocity between the gas in the Hill radius and the SMBH is expressed as  $\Delta v = \Omega_K R_{\text{hill}}/2 = 7.1 \times 10^7 \text{ cm s}^{-1}$ , which is comparable with the sound speed and not considered in this case just for a rough estimation. Finally the gas mass within the Hill radius is  $M_{\text{Bon}} = 2\pi H_p R_{\text{hill}}^2 \rho_p/3 = 1.3 \times 10^{-4} M_\odot \ll M_s$ , indicating that the enhancement effect from the self-gravity of Bondi sphere gas is marginal.

The outer radius of SMBH-disk  $X_{\text{out}}$  can be estimated through the conservation of AM based on Equation (A1). By setting  $\Delta R = R_{\text{hill}}$ , we derive

$$X_{\text{out}} = \frac{R_{\text{hill}}^4 M_p}{4R^3 M_s} = 1.8 \times 10^{11} r_1 M_8 q_5^{1/3} \text{ cm}. \quad (41)$$

This corresponds to  $1.2 \times 10^3 r_g$ . With Equation (A2), the accretion fraction  $f_{\text{acc}} \approx 6.9 \times 10^{-2}$  is obtained. With Equation (4), the conversion efficiency  $\eta_{\text{out}} \approx 6.9 \times 10^{-4}$  is derived. Like the middle region case, the turbulence scale  $l_{\text{turb}} \sim \alpha H_p \sim 0.1 H_p$  is much smaller than the size of accretion region  $\min\{R_{\text{Bon}}, R_{\text{hill}}, H_p\} = H_p$ , so the uncertainty of  $f_{\text{acc}}$  introduced by turbulence can be ignored. Based on Equation (3) and (39), the power of the outflow is given by

$$L_{\text{out}} \approx 4.9 \times 10^{43} \eta_3 \alpha_{0.1}^{-1} r_1 M_8 q_5^{1/3} \text{ erg s}^{-1}, \quad (42)$$

where  $\eta_3 = \eta_{\text{out}}/10^{-3}$ .

Based on Equations (5) and (42), the cavity radius is derived  $R_{\text{cav}} = 1.3 \times 10^{13} \text{ cm}$ . The derived cavity radius is much larger than the SMBH-disk half-thickness, which indicates that the outflow can significantly change the local disk structure. In this case, the maximum of cavity radius is

$$R_{\text{cav}} = H_p = 1.2 \times 10^{12} M_8 \dot{M}_p \text{ cm}. \quad (43)$$

The gas mass within the cavity volume is  $M_{\text{cav}} = 4\pi R_{\text{cav}}^3 \rho_p/3 = 8.0 \times 10^{-5} M_\odot$ . When the accretion is halted, the outflow radius is  $R_{\text{out}} = \min\{R_{\text{Bon}}, R_{\text{hill}}, H_p, R_{\text{cav}}\} = H_p = 1.2 \times 10^{12} \text{ cm}$  and the outflow mass is  $M_{\text{out}} = 4\pi R_{\text{out}}^3 \rho_p/3 = 8.0 \times 10^{-5} M_\odot$ . Using equations (8), (9), and (42), we obtain the velocity of the outflow and the cavity expansion time

$$v_{\text{out}} = 9.1 \times 10^8 \eta_3^{1/3} r_1^{-1/6} q_5^{1/9} \text{ cm s}^{-1}, \quad (44)$$

$$t_{\text{out}} = 1.4 \times 10^3 \eta_3^{-1/3} r_1^{1/6} \dot{M}_p M_8 q_5^{-1/9} \text{ s}. \quad (45)$$

The energy of outflows is  $E_{\text{out}} = L_{\text{out}} t_{\text{out}} = 6.6 \times 10^{46}$  erg. We calculate the energy required to do work against the external pressure and the AMS gravity. First, the energy used to overcome the pressure of the SMBH-disk is  $E_p = 4\pi P R_{\text{out}}^3/3 = 1.0 \times 10^{45}$  erg. Second, the energy used to overcome the gravity of the AMS is  $E_g = G M_{\text{out}} M_s / R_{\text{out}} = 1.7 \times 10^{46}$  erg. These two kinds of energies are much smaller than the outflow energy  $E_{\text{out}}$ , indicating that the influence of SMBH-disk pressure and AMS gravity on the outflow expansion could be ignored. We also calculate the initial mass of outflows  $M_{\text{ini}} \approx (1 - f_{\text{acc}}) \dot{M}_s t_{\text{out}} = 3.4 \times 10^{-5} M_{\odot} \lesssim M_{\text{out}}$ , which verifies the validity of former approximation of ignoring it in Equations (44) and (45).

The velocity of outflow is about one order of magnitude larger than the sound speed, which inevitably leads to the formation of shock when the outflow collides with the surrounding gas medium. The powerful shock would accelerate the thermal electrons to relativistic state, which give rise to the non-thermal emissions due to the synchrotron radiation and inverse Compton scattering processes, as can be seen in Figure 4. In the meanwhile, the shock will also heat the SMBH-disk gas with an extremely high temperature of  $T_{\text{sh}} = 1.9 \times 10^9$  K, given by Equations (10) and (44). This can lead to the generation of relativistic jet if the SMBH is rapidly spinning (Rees et al. 1982). Using the pressure equilibrium condition between the shocked gas and SMBH-disk based on Equation (11), we derive the density of shocked gas  $\rho_{\text{sh}} = 8.0 \times 10^{-10} \text{ g cm}^{-3}$ , much lower than the density of the SMBH-disk gas. With Equation (12), the cooling timescale of the shocked gas can be derived  $t_{\text{cool}} = 16.4 \text{ s}$ , much shorter than the cavity expansion timescale, which implies that the free-free cooling mechanism is very efficient.

After the hot gas in the cavity is cooled quickly, the cavity, based on Equations (13) and (43), will be refilled in a rejuvenation timescale of

$$t_{\text{rej}} = 1.8 \alpha_{0.1}^{-1} r_1^{3/2} M_8 \text{ d}, \quad (46)$$

much longer than the cavity formation timescale. Based on Equations (A17), (A18), and (41), the radial velocity and the viscosity timescale of the SMBH-disk are derived,

$$v_r = 3.4 \times 10^7 \alpha_{0.1} r_1^{-1/2} q_5^{1/3} \text{ cm s}^{-1}, \quad (47)$$

$$t_{\text{vis}} = 1.5 \alpha_{0.1}^{-1} r_1^{3/2} M_8 \text{ hr}. \quad (48)$$

The viscosity timescale is much longer than the expansion timescale  $t_{\text{out}}$ . This means that after the outflows rush out of the SMBH-disk, the accretion onto AMS still continues and lasts for a timescale of  $t_{\text{last}} = t_{\text{vis}}$ . The duty cycle of the accretion process is  $\delta = t_{\text{last}} / (t_{\text{last}} + t_{\text{rej}}) = 4.2 \times 10^{-2}$ . The average dimensionless net mass accretion rate of the SMBH is  $\dot{\mathcal{M}}_{\text{ave}} = f_{\text{acc}} \delta \dot{\mathcal{M}}_s = 1.1 \times 10^3$ , which indicates that mass growing timescale of SMBH is much shorter than the Salpeter time  $t_{\text{Salp}} = M_s / \dot{M}_{\text{Edd}} = 0.45 \text{ Gyr}$ . However, the SMBH in the inner region will merge with the SMBH quickly due to the gravitational wave radiation (see Equation 24 in Wang et al. 2023a), which avoids that the SMBH mass grows to be too large. After the SMBH-disk is consumed, the cavity will quickly cool in a timescale of  $t_{\text{cool}}$  and accretion process restarts.

## 4. OBSERVATION SIGNATURES

### 4.1. Thermal emission

Now we calculate the thermal light curves of Bondi explosion. The diffusion timescale of the photons is given by  $t_{\text{diff}} = \kappa M_{\text{ej}} / \beta_0 c R_{\text{cav}}$ , where  $M_{\text{ej}} = M_{\text{cav}}$  is the ejecta mass, and a value of  $\beta_0 = 13.7$  is utilized to accommodate various density profiles of the diffusion mass (Arnett 1982). For AMS in the outer region, we set  $\kappa = 1.0$  for simplicity, ignoring its complex dependence on the radius, as shown in Figure 5. For AMSs in the middle and inner regions, the opacity is determined by electron scattering and  $\kappa = 0.4$ . Since the post-shock medium is quite hot ( $T_{\text{sh}} \sim 10^5, 10^8, 10^9$  K in the outer, middle, and inner regions, respectively), free-free absorption, bound-free and bound-bound absorption could be not important in the main phase of the Bondi explosion. We may include these effects for later phase of the explosion. The cavity expands with a timescale of  $t_{\text{out}}$ , which is much shorter than the diffusion timescale, as indicated in Table 2. Therefore, an effective light curve timescale  $t_{\text{eff}} = \sqrt{2 t_{\text{diff}} t_{\text{out}}}$  is introduced (Chatzopoulos et al. 2012). The electromagnetic emissions from the Bondi explosion will emerge within the timescale of  $t_{\text{eff}}$ . We calculate the thermal light curves for a simple form of the input luminosity  $L_{\text{inp}} = L_{\text{out}} \theta(t_{\text{last}} - t)$ , where  $\theta(t_{\text{last}} - t)$  denotes the Heaviside step function. More detailed interaction processes between the outflows and SMBH-disk gas, such as the reverse and forward shock, are beyond the scope of this study. The output luminosity of the homologously expanding photosphere is described by Equation (3) in Chatzopoulos et al. (2012),

$$L_{\text{bol}}(t) = \frac{2}{t_{\text{eff}}} \exp\left(-\frac{t^2}{t_{\text{eff}}^2} - \frac{2R_{\text{out}}t}{v_{\text{out}}t_{\text{eff}}^2}\right) \int_0^t \left(\frac{R_{\text{out}}}{v_{\text{out}}t_{\text{eff}}} + \frac{t'}{t_{\text{eff}}}\right) \exp\left(\frac{t'^2}{t_{\text{eff}}^2} + \frac{2R_{\text{out}}t'}{v_{\text{out}}t_{\text{eff}}^2}\right) L_{\text{inp}}(t') dt'. \quad (49)$$

**Table 2.** Explanations and typical values of some key parameters.

Parameters	Symbols	Inner	Middle	Outer
Parameters of the SMBH-disk.				
sMBH locus	$R/(R_g)$	10	$10^3$	$10^5$
sMBH mass	$M_s/(M_\odot)$	$10^3$	$10^3$	$10^2$
Magnetic field	$B/(G)$	$5.7 \times 10^4$	$2.5 \times 10^2$	25.2
Opacity	$\kappa/(\text{cm}^2 \text{g}^{-1})$	0.4	0.4	1.0
Parameters of the sMBH-disk.				
Size	$X_{\text{out}}/(r_g)$	$1.2 \times 10^3$	$1.2 \times 10^5$	$7.9 \times 10^6$
Viscosity timescale	$t_{\text{vis}}/(\text{d})$	$6.3 \times 10^{-2}$	62.6	$3.2 \times 10^3$
Parameters of the outflows.				
Luminosity of the inverse Compton scattering	$L_{\text{IC}}/(\text{erg s}^{-1})$	$4.9 \times 10^{42}$	$2.2 \times 10^{43}$	$6.3 \times 10^{41}$
Expansion timescale	$t_{\text{out}}/(\text{d})$	$1.6 \times 10^{-2}$	1.5	$6.3 \times 10^3$
Lasting time	$t_{\text{last}}/(\text{d})$	$6.3 \times 10^{-2}$	62.6	$6.3 \times 10^3$
Radius	$R_{\text{out}}/(\text{cm})$	$1.2 \times 10^{12}$	$3.6 \times 10^{13}$	$6.2 \times 10^{15}$
Parameters of the non-thermal electrons.				
Number density	$N_0/(\text{cm}^{-3})$	$2.5 \times 10^8$	$2.6 \times 10^8$	13.4
The maximum of Lorentz factor	$\gamma_{\text{max}}$	$3.3 \times 10^3$	$1.6 \times 10^4$	$2.0 \times 10^3$
The minimum of Lorentz factor	$\gamma_{\text{min}}$	1	1	1
The power-law index	$p_e$	2	2	2
Parameters of the thermal light curves.				
Ejecta mass	$M_{\text{ej}}/(M_\odot)$	$8.0 \times 10^{-5}$	0.34	$2.4 \times 10^2$
Diffusion timescale	$t_{\text{diff}}/(\text{d})$	1.4	$2.1 \times 10^2$	$6.0 \times 10^2$
Effective light curve timescale	$t_{\text{eff}}/(\text{d})$	0.21	24.9	$2.8 \times 10^3$
Peak luminosity	$L_{\text{peak}}/(\text{erg s}^{-1})$	$6.0 \times 10^{42}$	$2.2 \times 10^{44}$	$6.3 \times 10^{42}$
Effective temperature	$T_{\text{eff}}/(\text{K})$	$2.7 \times 10^5$	$1.2 \times 10^5$	$2.0 \times 10^3$

The initial radius is set as the outflow radius  $R_{\text{out}}$ , and the initial internal energy can be disregarded.

We then obtain the light curves of the thermal emission,

$$L_{\text{bol}}(t) = \begin{cases} L_{\text{out}} \left[ 1 - \exp\left(-\frac{t^2}{t_{\text{eff}}^2} - \frac{2R_{\text{out}}t}{v_{\text{out}}t_{\text{eff}}^2}\right) \right], & t < t_{\text{last}}, \\ L_{\text{out}} \left[ \exp\left(\frac{t_{\text{last}}^2}{t_{\text{eff}}^2} + \frac{2R_{\text{out}}t_{\text{last}}}{v_{\text{out}}t_{\text{eff}}^2}\right) - 1 \right] \exp\left(-\frac{t^2}{t_{\text{eff}}^2} - \frac{2R_{\text{out}}t}{v_{\text{out}}t_{\text{eff}}^2}\right), & t > t_{\text{last}}, \end{cases} \quad (50)$$

which exhibit an increase over a timescale of  $t_{\text{last}}$  and a Gaussian decay over the effective light curve timescale  $t_{\text{eff}}$ . The luminosity reaches its peak after a time interval of  $t_{\text{last}}$  as  $L_{\text{peak}} = L_{\text{out}}[1 - \exp(-t_{\text{last}}^2/t_{\text{eff}}^2 - 2R_{\text{out}}t_{\text{last}}/v_{\text{out}}t_{\text{eff}}^2)]$ , the detailed calculated results of which are listed in Table 2.

Due to the highly effective free-free cooling of the hot gas within the cavity, the expanding shell loses its energy in the form of black body radiation with an effective temperature  $T_{\text{eff}} = (L_{\text{peak}}/4\pi R_{\text{cav}}^2 \sigma_{\text{SB}})^{1/4}$ , where  $\sigma_{\text{SB}}$  is Stefan-Boltzmann constant. The black body spectra are plotted in purple (see Figures 2-4). The thermal luminosity  $L_{\text{peak}} \approx 10^{43} \text{ erg s}^{-1}$  of Bondi explosion in the outer region peaks in the infrared band, slightly higher than that of the AGN-disk. In the middle region, the thermal luminosity of  $L_{\text{peak}} \approx 10^{44} \text{ erg s}^{-1}$  of Bondi explosion greatly exceed that of the SMBH-disk in the UV band. While the Bondi explosions occurring in the inner region could lead to soft X-ray flares with a luminosity of  $L_{\text{peak}} \approx 10^{43} \text{ erg s}^{-1}$ .

#### 4.2. Non-thermal emissions

As discussed in § 3, the velocity of the outflows exceeds the local sound speed, leading to the development of shocks (Blandford & Eichler 1987) and the generation of non-thermal electrons and emissions (Amano et al. 2022). Following the approach of



Inoue & Takahara (1996) and utilizing a simplified homogeneous one-zone model framework, we compute the broad band SED of synchrotron radiation and inverse Compton (IC) scattering. It is worth noting that unlike the jet case, there is no beaming effect in the case of outflows, and thus the beaming factor is set to unity.

The thermal electrons are accelerated to a relativistic state due to shock acceleration (see e.g., Drury 1983; Blandford & Eichler 1987). The acceleration timescale is given by  $t_{\text{acc}} = 20\xi_{\text{acc}}R_Lc/3v_{\text{out}}^2$  (Inoue & Takahara 1996), where  $R_L = \gamma m_e c^2 / eB$  denotes the Larmor radius,  $m_e$  is the electron mass, and  $\xi_{\text{acc}}$  is a factor characterizing the acceleration efficiency that depends on the acceleration environment. For instance,  $\xi_{\text{acc}} \sim 1$  (referred to as the ‘‘Borm limit’’) in supernova remnant (Uchiyama et al. 2007), while in blazars,  $\xi_{\text{acc}}$  can reach up to  $10^7$  (Inoue & Takahara 1996). In the context of AMS, where the shock is not relativistic, we take  $\xi_{\text{acc}} \sim 1$ . The magnetic field is derived as  $B = (32\pi a/3)^{1/2}T_c^2$ , under the assumption of equipartition with the radiation energy density (Burbidge 1956), where  $a = 4\sigma_T/c$  is the black body radiation constant. Note that the midplane temperature  $T_c$  in the outer region of AGN disk is approximately a constant  $10^4$  K (see Figure 5). The non-thermal electrons lose their energy due to inverse Compton scattering in a cooling timescale of  $t_{\text{IC}} = 3m_e c / 4\sigma_T \gamma u_{\text{ph}}$ , where  $\gamma$  is the Lorentz factor of the non-thermal electrons, and  $u_{\text{ph}} = aT_c^4$  is the energy density of the local seed photons radiated by the SMBH-disk. By utilizing the condition  $t_{\text{acc}} = t_{\text{IC}}$ , we derive the maximum Lorentz factor  $\gamma_{\text{max}}$ . The energy spectrum of the non-thermal electrons is given by  $dN/d\gamma = (1 - p_e)N_0\gamma^{-p_e} / (\gamma_{\text{max}}^{1-p_e} - \gamma_{\text{min}}^{1-p_e})$ , where  $N_0$  is the total number density obtained by integrating  $dN/d\gamma$  from  $\gamma_{\text{min}}$  to  $\gamma_{\text{max}}$ . Here, we set  $\gamma_{\text{min}} = 1$  and the spectral index  $p_e = 2$ .

Now we calculate the SED of the non-thermal radiation. First, we consider the inverse Compton scattering, where the photons from the SMBH-disk are scattered by the non-thermal electrons and transformed into  $\gamma$ -rays. By setting the inverse Compton scattering luminosity as  $L_{\text{IC}} = \zeta L_{\text{out}}$ , we can derive the number density of the non-thermal electrons  $N_0$ . Here, the parameter  $\zeta$  representing the typical fraction of non-thermal emissions generated by shocks is quite uncertain (e.g., Blandford & Eichler 1987), so we set  $\zeta \sim 0.1$ . The number density of the seed photons is estimated as  $n_\nu = 4\pi B_\nu / h\nu c$ , where  $B_\nu = 2h\nu^3/c^2(\exp(h\nu/k_B T_c) - 1)$  is the black body spectrum. Subsequently, we calculate the SEDs of the synchrotron radiation with the magnetic field  $B$  and number density of non-thermal electrons  $N_0$ . The calculated SEDs of the inverse Compton scattering and synchrotron radiation are plotted in Figures 2-4, with parameters listed in Table 2.

## 5. DISCUSSION

AMSs in the inner (middle) regions display quasi-periodic eruptions (QPEs) with a duration of several hours (months) and a period of several days (years), providing valuable insights into the QPE with various periods (e.g., Evans et al. 2023; Guolo et al. 2024). In fact, the AMS model has been applied to Sgr A\* (Wang et al. 2023a), successfully explaining its quasi-periodic flickerings observed in the near-infrared band.

The light curves of thermal luminosity for Bondi explosions occurring in different regions of SMBH-disk exhibit a broad range of duration timescales, spanning from several hours to decades at different bands from infrared to soft X-ray band. In the outer region, the diffusion timescale of Bondi explosion is much shorter than the expansion timescale, causing the light curve to behave like the Heaviside step function, as shown in Figure 2. The thermal luminosity can be estimated as  $L_{\text{bol}}(t) \approx L_{\text{out}}$  and lasts for a time interval of decades. Thermal luminosity of Bondi explosions occurring in the middle region exhibit a slow rise and rapid decay (see Figure 3). Conversely, in the inner region, the thermal luminosity of Bondi explosion experiences a rapid rise and slow decay (see Figure 4). These diverse and intriguing features show that AMSs could be accountable for astronomical transients of varying durations. Indeed, various atypical transients have been documented in recent years. For example, Ofek et al. (2021) reported an optical transient, AT 2018lqh, with a duration on the scale of days attributed to an explosion of low-mass ejecta ( $\approx 0.07 M_\odot$ ), which is comparable to those of the AMS in middle region if the sMBH mass and its location are appropriately adjusted. While in X-ray band, Khamitov et al. (2023) presented an SRG/eROSITA X-ray catalog with significant proper motions explained by the presence of transient events, supporting the idea of AMSs being the possible physical origin of these transient events.

The SEDs of Bondi explosions occurring in different regions of the SMBH-disk exhibit various features. The synchrotron radiations of AMS in the outer region could span from  $\sim 10$  GHz to optical bands. The ratio of radio to optical luminosity is  $\sim 10^{-5}$ , which could explain part of radio emissions of radio-quiet AGNs. Recent radio sky surveys, such as the Very Large Array Sky Survey (VLASS, Gordon et al. 2021) at 2-4 GHz, and the LOw-Frequency ARray (LOFAR) Two-metre Sky Survey (Shimwell et al. 2022) at 120-168 MHz, can be helpful to search for radio transients from Bondi explosion. These catalogs are compared with older sky surveys, such as the NRAO VLA Sky Survey (NVSS, Condon et al. 1998), the Sydney University Molonglo Sky Survey (SUMSS, Mauch et al. 2003), and Faint Images of the Radio Sky at Twenty Centimeters (FIRST, Helfand et al. 2015), to study the long timescale radio variability (Nyland et al. 2020). In fact, long-term radio variability (e.g., Hovatta et al. 2008; Park & Tripp 2017; Zhang et al. 2022) and some radio transients from, such as the Caltech-NRAO Stripe 82 Survey



(CNSS, Mooley et al. 2016) with variability timescales between 1 week and 1.5 yr, the Variables and Slow Transients Survey (VAST) on the Australian Square Kilometre Array Pathfinder (ASKAP, Murphy et al. 2021) with variability timescales from 5 s to 5 yr, have been reported for a considerable number of AGNs. These radio transients events are very helpful to search for the AMSs.

Another interesting feature of the AMS SED is the high-energy  $\gamma$ -ray photons (peaked from approximately 10 MeV to GeV). For AMSs located in the middle regions of the SMBH-disk, the  $\gamma$ -ray luminosity is estimated to be around  $10^{43} \text{ erg s}^{-1}$ , corresponding to a flux of  $3.7 \times 10^{-13} \text{ erg s}^{-1} \text{ cm}^{-2}$  for a nearby AGN with redshift  $z = 0.1$ , which is comparable with the sensitivity of the Fermi/LAT at the GeV band with 10 years of observation<sup>1</sup>. It is worth noting that the  $\gamma$ -ray luminosity is determined by several physical parameters, for example, as described in Equations (30) and (31), a higher sMBH mass results in a shorter size of the sMBH-disk and more powerful outflows, leading to higher  $\gamma$ -ray luminosity and flux. On the other hand, the stacking technique of  $\gamma$ -rays presented in Paliya et al. (2019) and Ajello et al. (2021) will be useful for detecting fainter  $\gamma$ -rays below the Fermi/LAT sensitivity. In fact, significant  $\gamma$ -ray detections have been reported for some nearby low-luminosity active galactic nuclei (LLAGN; de Menezes et al. 2020). It is easy for the AMSs to outshine from the LLAGN, although SMBHs in LLAGN generally accrete with low, sub-Eddington accretion rates (Ho 2008) that would influence the AMS luminosity (see Equations 20, 31, and 42).

## 6. CONCLUSION

In this study, we investigate the accretion-modified stars (AMS) embedded in different regions of the disk surrounding the supermassive black holes (SMBHs), namely the inner region (typical radius  $R = 10 R_g$ ), the middle region (typical radius  $R = 10^3 R_g$ ), and the outer region (typical radius  $R = 10^5 R_g$ ). In the inner and middle regions, the Toomre parameter  $Q > 1$ , and the standard model (Shakura & Sunyaev 1973) is utilized. In the outer region,  $Q \approx 1$ , the self-gravitating disk model (Goodman 2003; Sirko & Goodman 2003) is employed. Bondi explosions in these regions exhibit both similarities and distinct characteristics, depending on various gas environment, primarily including gas density, sound speed, and half-thickness of the SMBH-disk. The main findings are summarized below:

(1): The main physical processes are similar for AMSs embedded in the inner and middle regions of the SMBH-disk. The AMS experiences hyper-Eddington accretion ( $\sim 10^6 - 10^7 L_{\text{Edd},s}/c^2$ ), resulting in the development of strong outflows that collide with the SMBH-disk, generating shocks, heating the SMBH-disk gas, accelerating electrons to relativistic state, and emitting non-thermal radiations. In the inner and middle regions, after the powerful outflow rushes out of the SMBH-disk, a cavity is formed, but it quickly cools and is then refilled by the surrounding cool gas of the SMBH-disk. While in the outer region, the inflows of Bondi accretion and outflows from Bondi explosion coexist and can last for several decades, as shown in Figure 1.

(2): We compute the thermal light curves for a constant input luminosity within the lasting timescale of the outflows. The results show that the flare of the Bondi explosion in the inner region displays fast rise and slow Gaussian decay, with a timescale of several hours and a luminosity of  $\sim 10^{43} \text{ erg s}^{-1}$  peaked at the soft X-ray band. While in the middle region, the Bondi explosion exhibits slow rise and rapid Gaussian decay, with a timescale of months and a luminosity of  $\sim 10^{44} \text{ erg s}^{-1}$  peaked at the UV band. In the outer region, the light curve of Bondi explosion resembles the Heaviside step function, lasting for decades and contributing a slightly higher luminosity of  $\sim 10^{43} \text{ erg s}^{-1}$  than the AGN disk itself in the infrared band. These light curves provide valuable insights into the diverse astronomical transient events associated with AGNs.

(3): We calculate the multiwavelength spectral energy distributions of the Bondi explosion from radio to  $\gamma$ -ray bands. The  $\gamma$ -rays luminosity of IC ranges from  $10^{42}$  to  $10^{43} \text{ erg s}^{-1}$  in the GeV (middle and inner regions) and 10 MeV (outer region) bands, respectively. Moreover, the radio emission due to synchrotron radiation from Bondi explosion occurring in the outer region can contribute to that of the radio-quiet AGNs or result in a long term radio variability over a timescale of several decades. The synchrotron radiation of Bondi explosion in the middle and inner regions peaks at the X-ray band with luminosities of  $\sim 10^{43}$  and  $\sim 10^{42} \text{ erg s}^{-1}$ , respectively.

<sup>1</sup> <https://www.slac.stanford.edu/exp/glast/groups/canda/lat.Performance.htm>

IHEP AGN Group members are acknowledged for useful discussions. Many thanks to Fu-Lin Li for useful discussions about the supernova light curve calculations. Jun-Rong Liu thanks the support by the National Key R&D Program of China through grant-2016YFA0400701 and -2020YFC2201400 by NSFC-11991050, -11991054, -11833008, -11690024, and by grant No. QYZDJ-SSW-SLH007 and No. XDB23010400. LCH was supported by the NSFC (11721303, 11991052, 12233001), the National Key R&D Program of China (2022YFF0503401), and the China Manned Space Project (CMS-CSST-2021-A04, CMS-CSST-2021-A06).

## APPENDIX

### A. HYPER-EDDINGTON ACCRETION DISK

In the region close to the sMBH, the falling gas will form a hyper-Eddington accretion disk (e.g., Wang et al. 2021a; Chen et al. 2023) since the differential rotation of gas leads to net angular momentum (AM). The outer radius of sMBH-disk  $X_{\text{out}}$  can be estimated through the conservation of AM. The specific net AM of the gas from differential rotation is given by  $\Delta\ell_p = (\Delta R)^2 \Omega_{K,s}/2$ , where  $\Delta R$  is the size of accretion region. The specific AM of the sMBH-disk is  $\Delta\ell_s = \sqrt{X_{\text{out}} GM_s}$ . By setting  $\Delta\ell_p = \Delta\ell_s$ , we derive

$$X_{\text{out}} = \frac{(\Delta R)^4 M_p}{4R^3 M_s}. \quad (\text{A1})$$

The sMBH-disk size strongly depends on  $\Delta R$ .

A radius-dependent accretion rate is often adopted in references,  $\dot{M} = \dot{M}_{\text{out}} (r/X_{\text{out}})^s$ , where  $\dot{M}_{\text{out}} = \mathcal{M}_s \dot{M}_{\text{Edd}}$  is the accretion rate at outer radius  $X_{\text{out}}$ , and  $r$  is the radius of the sMBH-disk. Index  $s$  ranges from 0 to 1, which is dependent on the ratio of the radiation energy to the dissipated gravitational energy (Begelman 2012). In purely adiabatic flows,  $s = 1$  (Begelman 2012).  $s$  can also be estimated by numerical result in different cases (e.g., Yang et al. 2014; Kitaki et al. 2021; Pan & Yang 2021; Cao & Gu 2022). For example, Yang et al. (2014) considered the effect the  $T_{\theta\phi}$  component of viscous stress in two dimensional simulation and found that  $s$  is in the range of  $\sim 0.4 - 1.0$ . In consideration of the above uncertainties, a moderate index  $s = 1/2$  is adopted in this work. So we have the fraction of the accretion rate onto the sMBH to the Bondi accretion rate

$$f_{\text{acc}} = \left( \frac{X_{\text{in}}}{X_{\text{out}}} \right)^{1/2}, \quad (\text{A2})$$

where  $X_{\text{in}} = 6 r_g$  is the inner radius of the sMBH-disk.

Based on equations (1)-(7) in Wang & Zhou (1999) but replacing  $\dot{M}$  with  $\dot{M}_{\text{out}} (r/X_{\text{out}})^s$ , the governing equations read

$$\dot{M}_{\text{out}} \left( \frac{r}{X_{\text{out}}} \right)^s = 4\pi r H_s \rho_s v_r, \quad (\text{A3})$$

$$\frac{P_s}{\rho_s} = H_s^2 \Omega_{K,s}^2, \quad (\text{A4})$$

$$\dot{M}_{\text{out}} \left( \frac{r}{X_{\text{out}}} \right)^s (l - l_{\text{in}}) = 4\pi r^2 H_s \alpha P_s, \quad (\text{A5})$$

$$\frac{1}{\rho_s} \frac{dP_s}{dr} - (\Omega^2 - \Omega_{K,s}^2) r + v_r \frac{dv_r}{dr} + \frac{P_s}{\rho_s} \frac{d \ln \Omega_{K,s}}{dr} = 0, \quad (\text{A6})$$

$$Q_{\text{adv}} = \frac{\dot{M}_{\text{out}}}{4\pi r^2} \left( \frac{r}{X_{\text{out}}} \right)^s \left( \frac{P_s}{\rho_s} \right) \xi, \quad (\text{A7})$$

$$Q_{\text{vis}} = \frac{n f \Omega^2 \dot{M}_{\text{out}}}{4\pi} \left( \frac{r}{X_{\text{out}}} \right)^s, \quad (\text{A8})$$

$$Q_{\text{adv}} = Q_{\text{vis}}, \quad (\text{A9})$$

$$P_s = \frac{a T_s^4}{3}, \quad (\text{A10})$$

where  $l = \Omega r^2$  is the specific AM,  $l_{\text{in}}$  is the specific AM at the inner boundary,  $\Omega_{K,s} = \sqrt{GM_s/r^3}$  is the Keplerian angular velocity of the sMBH-disk,  $\xi = (4 - 0.75\beta)\gamma_\rho - (12 - 10.5\beta)\gamma_T$ ,  $\beta \ll 1$  is the ratio of gas to total pressure,  $\gamma_\rho = d \ln \rho_s / d \ln r$ ,  $\gamma_T = d \ln T_s / d \ln r$ ,  $n = -d \ln \Omega / d \ln r$ ,  $f = 1 - l_{\text{in}}/l$ , and  $a$  is the black body radiation constant. Note that the coefficients  $B_i$  in Muchotrzeb & Paczynski (1982) are around unit and can be disregarded following Wang & Zhou (1999). There are 8 equations of the sMBH-disk to determine 8 free physical quantities, i.e., total pressure  $P_s$ , density  $\rho_s$ , radial velocity  $v_r$ , disk half-thickness  $H_s$ , angular velocity  $\Omega$ , advection cooling rate  $Q_{\text{adv}}$ , energy generation per area  $Q_{\text{vis}}$ , and temperature  $T_s$ .

The boundary condition of zero-torque at the inner edge of the disk is adopted here. By combining Equations (A3)-(A10), we then derive the self-similar solutions of hyper-Eddington disk with outflows,

$$P_s = \left( \frac{\xi f}{n} \right)^{1/2} \frac{\Omega_{K,s} \dot{M}_{\text{out}}}{4\pi \alpha r} \left( \frac{r}{X_{\text{out}}} \right)^s \propto r^{s-5/2}, \quad (\text{A11})$$

$$\rho_s = \frac{\gamma_0^2}{4\pi \alpha} \left( \frac{\xi^3}{n^3 f} \right)^{1/2} \frac{\dot{M}_{\text{out}}}{\Omega_{K,s} r^3} \left( \frac{r}{X_{\text{out}}} \right)^s \propto r^{s-3/2}, \quad (\text{A12})$$

$$v_r = \frac{n \alpha}{\xi \gamma_0} r \Omega_{K,s} \propto r^{-1/2}, \quad (\text{A13})$$

$$H_s = \frac{r}{\gamma_0} \left( \frac{n f}{\xi} \right)^{1/2} \propto r, \quad (\text{A14})$$

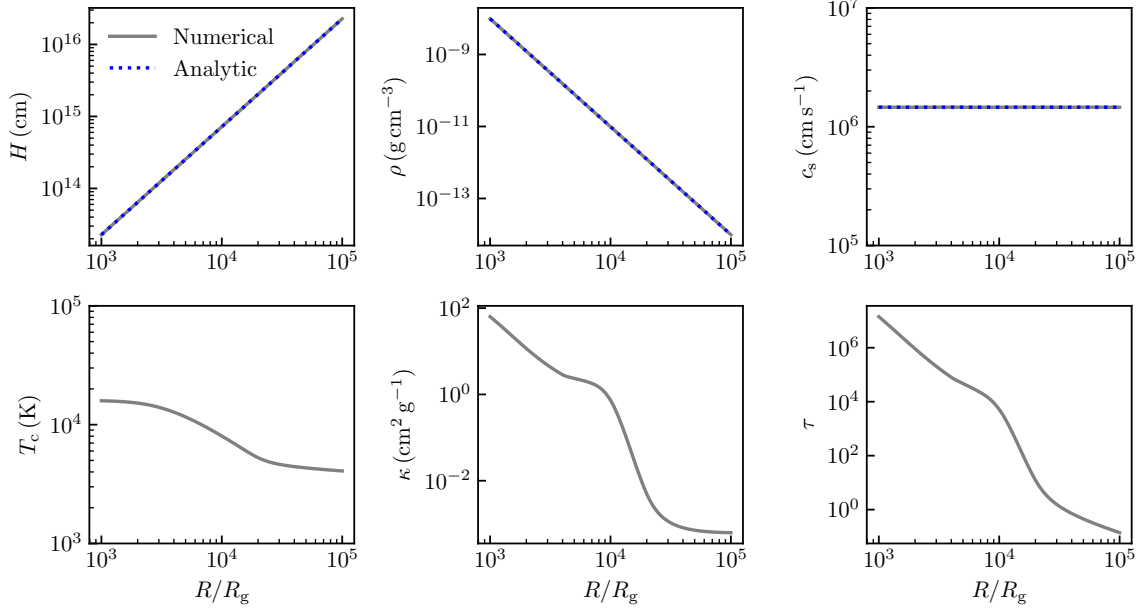


**Figure 5.** The parameters of the self-gravitating disk for given  $M_8 = 1$ ,  $\dot{M}_p = 1$ ,  $\alpha = 0.1$ , and  $b = 0$ . The blue dotted lines are analytic solutions described by Equations (B31)-(B33). The gray lines are numerical solutions derived from Equations (B19)-(B30).

$$\Omega = \frac{\Omega_{K,s}}{\gamma_0} \propto r^{-3/2}, \quad (\text{A15})$$

$$T_s = \left(\frac{\xi f}{n}\right)^{1/8} \left(\frac{3\dot{M}_{\text{out}}\Omega_{K,s}}{4\pi a \alpha r}\right)^{1/4} \left(\frac{r}{X_{\text{out}}}\right)^{s/4} \propto r^{s/4-5/8}, \quad (\text{A16})$$

where  $\gamma_p = d \ln \rho_s / d \ln r = s - 3/2$ ,  $\gamma_T = d \ln T_s / d \ln r = s/4 - 5/8$ ,  $n = -d \ln \Omega / d \ln r = 3/2$ ,  $\gamma_0 = [1 - n f(\gamma_p - 3/2)/\xi - n^2 \alpha^2 \gamma_v / \xi^2]$ ,  $\gamma_p = d \ln P_s / d \ln r = s - 5/2$ ,  $\gamma_v = d \ln v_r / d \ln r = -1/2$ . By setting  $r = X_{\text{out}}$ , the radial velocity  $v_r$  and viscosity timescale of the SMBH-disk can be estimated

$$v_r \approx \frac{1}{25} \sqrt{\frac{GM_s}{X_{\text{out}}}}, \quad (\text{A17})$$

$$t_{\text{vis}} = \frac{X_{\text{out}}}{v_r}. \quad (\text{A18})$$

## B. SELF-GRAVITATING ACCRETION DISK

In the outer part of the AGN disk, the accretion disk becomes self-gravity dominated (Toomre 1964). We consider the regions where the Toomre parameter  $Q \sim 1$ . The basic equations read (Goodman 2003; Sirko & Goodman 2003),

$$\rho_p = \frac{\Omega^2}{2\pi G Q}, \quad (\text{B19})$$

$$\beta^b c_s^2 \Sigma_p = \frac{\dot{M}_p \Omega}{3\pi \alpha}, \quad (\text{B20})$$

$$\Sigma_p = 2\rho_p H_p, \quad (\text{B21})$$

$$H_p = \frac{c_s}{\Omega}, \quad (\text{B22})$$

$$T_c^4 = \left(\frac{3\tau}{8} + \frac{1}{2} + \frac{1}{4\tau}\right) T_{\text{eff}}^4, \quad (\text{B23})$$

$$\tau = \frac{\kappa \Sigma_p}{2}, \quad (\text{B24})$$

$$p_{\text{rad}} = \frac{\tau \sigma_{\text{SB}} T_{\text{eff}}^4}{2c}, \quad (\text{B25})$$

$$p_{\text{gas}} = \frac{\rho_p k_B T_c}{m}, \quad (\text{B26})$$

$$\beta = \frac{p_{\text{gas}}}{p_{\text{gas}} + p_{\text{rad}}}, \quad (\text{B27})$$

$$c_s^2 = \frac{p_{\text{gas}} + p_{\text{rad}}}{\rho_p}, \quad (\text{B28})$$

$$\kappa = \kappa(\rho_p, T_c), \quad (\text{B29})$$

$$\dot{M}_p = -2\pi R v_r' \Sigma_p, \quad (\text{B30})$$

where  $\Omega = \sqrt{GM_p/R^3}$  is the Keplerian angular velocity, and  $\sigma_{\text{SB}}$  is Stefan-Boltzmann constant, and  $m = 0.62 m_{\text{H}}$  is the mean molecular mass. We add the mass conservation equation (B30) compared with Sirko & Goodman (2003) to compute the radial velocity  $v_r'$ . The parameter  $b = 0$  ( $b = 1$ ) means that the viscosity is proportional to total (gas) pressure. For given mass accretion rate  $\dot{M}_p$ , viscosity parameter  $\alpha$ , SMBH mass  $M_p$ , radius  $R$ , minimum Toomre parameter  $Q_{\text{min}}$ , and  $b$ , these 12 equations can be solved to derive the 12 unknown parameters, gas density  $\rho_p$ , midplane temperature  $T_c$ , optical depth  $\tau$ , effective temperature  $T_{\text{eff}}$ , opacity  $\kappa$ , surface density  $\Sigma_p$ , fraction of gas pressure  $\beta$ , sound speed  $c_s$ , radiation pressure  $p_{\text{rad}}$ , gas pressure  $p_{\text{gas}}$ , disk half-thickness  $H_p$ , and radial velocity  $v_r'$ .

In this paper,  $b = 0$  is considered, i.e., the viscosity proportional to total pressure. For given  $\dot{M}_p$ ,  $\alpha$ ,  $M_p$ ,  $R$ , and  $Q_{\min} = 1$ , the solutions of  $H_p$ ,  $\rho_p$ ,  $c_s$ , and  $\Sigma_p$  can be derived by combining Equations (B19)-(B22),

$$H_p = \frac{\dot{M}_p^{1/3} R^{3/2}}{(3\alpha)^{1/3} G^{1/6} M_p^{1/2}}, \quad (\text{B31})$$

$$\rho_p = \frac{M_p}{2\pi R^3}, \quad (\text{B32})$$

$$c_s = \left( \frac{G \dot{M}_p}{3\alpha} \right)^{1/3}, \quad (\text{B33})$$

$$\Sigma_p = \frac{M_p^{1/2} \dot{M}_p^{1/3}}{\pi (3\alpha)^{1/3} G^{1/6} R^{3/2}}. \quad (\text{B34})$$

Based on Equation (B30) and the solution of surface density (Equation B34), the radial velocity  $v'_r$  is derived,

$$v'_r = \frac{(3\alpha)^{1/3} G^{1/6} \dot{M}_p^{2/3} R^{1/2}}{2M_p^{1/2}}. \quad (\text{B35})$$

The remaining 7 parameters,  $T_c$ ,  $\tau$ ,  $T_{\text{eff}}$ ,  $\kappa$ ,  $\beta$ ,  $p_{\text{rad}}$ , and  $p_{\text{gas}}$ , can be obtained using the above solutions and Equations (B23)-(B29). The key physical quantity, opacity  $\kappa$  determined by the temperature and density of the disk gas, can not be expressed analytically (Alexander & Ferguson 1994). So we derive their numerical solutions and plot them in Figure 5.

## REFERENCES

- Abbott, R., Abbott, T. D., Abraham, S., et al. 2020, *PhRvL*, 125, 101102, doi: [10.1103/PhysRevLett.125.101102](https://doi.org/10.1103/PhysRevLett.125.101102)
- Ajello, M., Baldini, L., Ballet, J., et al. 2021, *ApJ*, 921, 144, doi: [10.3847/1538-4357/ac1bb2](https://doi.org/10.3847/1538-4357/ac1bb2)
- Alexander, D. R., & Ferguson, J. W. 1994, *ApJ*, 437, 879, doi: [10.1086/175039](https://doi.org/10.1086/175039)
- Ali-Dib, M., & Lin, D. N. C. 2023, *MNRAS*, 526, 5824, doi: [10.1093/mnras/stad2774](https://doi.org/10.1093/mnras/stad2774)
- Amano, T., Matsumoto, Y., Bohdan, A., et al. 2022, *Reviews of Modern Plasma Physics*, 6, 29, doi: [10.1007/s41614-022-00093-1](https://doi.org/10.1007/s41614-022-00093-1)
- Arnett, W. D. 1982, *ApJ*, 253, 785, doi: [10.1086/159681](https://doi.org/10.1086/159681)
- Artymowicz, P., Lin, D. N. C., & Wampler, E. J. 1993, *ApJ*, 409, 592, doi: [10.1086/172690](https://doi.org/10.1086/172690)
- Ashton, G., Ackley, K., Hernandez, I. M., & Piotrkowski, B. 2021, *Classical and Quantum Gravity*, 38, 235004, doi: [10.1088/1361-6382/ac33bb](https://doi.org/10.1088/1361-6382/ac33bb)
- Bartos, I., Kocsis, B., Haiman, Z., & Márka, S. 2017, *ApJ*, 835, 165, doi: [10.3847/1538-4357/835/2/165](https://doi.org/10.3847/1538-4357/835/2/165)
- Begelman, M. C. 2012, *MNRAS*, 420, 2912, doi: [10.1111/j.1365-2966.2011.20071.x](https://doi.org/10.1111/j.1365-2966.2011.20071.x)
- Blandford, R., & Eichler, D. 1987, *PhR*, 154, 1, doi: [10.1016/0370-1573\(87\)90134-7](https://doi.org/10.1016/0370-1573(87)90134-7)
- Bondi, H. 1952, *MNRAS*, 112, 195, doi: [10.1093/mnras/112.2.195](https://doi.org/10.1093/mnras/112.2.195)
- Boyce, H., Haggard, D., Witzel, G., et al. 2022, *ApJ*, 931, 7, doi: [10.3847/1538-4357/ac6104](https://doi.org/10.3847/1538-4357/ac6104)
- Burbidge, G. R. 1956, *ApJ*, 124, 416, doi: [10.1086/146237](https://doi.org/10.1086/146237)
- Burleigh, K. J., McKee, C. F., Cunningham, A. J., Lee, A. T., & Klein, R. I. 2017, *MNRAS*, 468, 717, doi: [10.1093/mnras/stx439](https://doi.org/10.1093/mnras/stx439)
- Cantiello, M., Jermyn, A. S., & Lin, D. N. C. 2021, *ApJ*, 910, 94, doi: [10.3847/1538-4357/abdf4f](https://doi.org/10.3847/1538-4357/abdf4f)
- Cao, X., & Gu, W.-M. 2022, *ApJ*, 936, 141, doi: [10.3847/1538-4357/ac8980](https://doi.org/10.3847/1538-4357/ac8980)
- Chatzopoulos, E., Wheeler, J. C., & Vinko, J. 2012, *ApJ*, 746, 121, doi: [10.1088/0004-637X/746/2/121](https://doi.org/10.1088/0004-637X/746/2/121)
- Chen, K., & Dai, Z.-G. 2024, *ApJ*, 961, 206, doi: [10.3847/1538-4357/ad0dfd](https://doi.org/10.3847/1538-4357/ad0dfd)
- Chen, K., Ren, J., & Dai, Z.-G. 2023, *ApJ*, 948, 136, doi: [10.3847/1538-4357/acc45f](https://doi.org/10.3847/1538-4357/acc45f)
- Chen, Y.-X., & Lin, D. N. C. 2023, *MNRAS*, 522, 319, doi: [10.1093/mnras/stad992](https://doi.org/10.1093/mnras/stad992)
- Cheng, K. S., & Wang, J.-M. 1999, *ApJ*, 521, 502, doi: [10.1086/307572](https://doi.org/10.1086/307572)
- Condon, J. J., Cotton, W. D., Greisen, E. W., et al. 1998, *AJ*, 115, 1693, doi: [10.1086/300337](https://doi.org/10.1086/300337)
- Davies, M. B., & Lin, D. N. C. 2020, *MNRAS*, 498, 3452, doi: [10.1093/mnras/staa2590](https://doi.org/10.1093/mnras/staa2590)
- de Menezes, R., Nemmen, R., Finke, J. D., Almeida, I., & Rani, B. 2020, *MNRAS*, 492, 4120, doi: [10.1093/mnras/staa083](https://doi.org/10.1093/mnras/staa083)
- Dittmann, A. J., Cantiello, M., & Jermyn, A. S. 2021, *ApJ*, 916, 48, doi: [10.3847/1538-4357/ac042c](https://doi.org/10.3847/1538-4357/ac042c)
- Dittmann, A. J., Dempsey, A. M., & Li, H. 2024, *ApJ*, 964, 61, doi: [10.3847/1538-4357/ad23ce](https://doi.org/10.3847/1538-4357/ad23ce)
- Drury, L. O. 1983, *Reports on Progress in Physics*, 46, 973, doi: [10.1088/0034-4885/46/8/002](https://doi.org/10.1088/0034-4885/46/8/002)
- Evans, P. A., Nixon, C. J., Campana, S., et al. 2023, *Nature Astronomy*, 7, 1368, doi: [10.1038/s41550-023-02073-y](https://doi.org/10.1038/s41550-023-02073-y)
- Fan, X., & Wu, Q. 2023, *ApJ*, 944, 159, doi: [10.3847/1538-4357/acb532](https://doi.org/10.3847/1538-4357/acb532)
- Frank, J., King, A., & Raine, D. J. 2002, *Accretion Power in Astrophysics: Third Edition*

- Genzel, R., Eisenhauer, F., & Gillessen, S. 2010, *Reviews of Modern Physics*, 82, 3121, doi: [10.1103/RevModPhys.82.3121](https://doi.org/10.1103/RevModPhys.82.3121)
- Genzel, R., Schödel, R., Ott, T., et al. 2003, *Nature*, 425, 934, doi: [10.1038/nature02065](https://doi.org/10.1038/nature02065)
- Goodman, J. 2003, *MNRAS*, 339, 937, doi: [10.1046/j.1365-8711.2003.06241.x](https://doi.org/10.1046/j.1365-8711.2003.06241.x)
- Gordon, Y. A., Boyce, M. M., O’Dea, C. P., et al. 2021, *ApJS*, 255, 30, doi: [10.3847/1538-4365/ac05c0](https://doi.org/10.3847/1538-4365/ac05c0)
- Graham, M. J., Ford, K. E. S., McKernan, B., et al. 2020, *PhRvL*, 124, 251102, doi: [10.1103/PhysRevLett.124.251102](https://doi.org/10.1103/PhysRevLett.124.251102)
- Graham, M. J., McKernan, B., Ford, K. E. S., et al. 2023, *ApJ*, 942, 99, doi: [10.3847/1538-4357/aca480](https://doi.org/10.3847/1538-4357/aca480)
- GRAVITY Collaboration, Bauböck, M., Dexter, J., et al. 2020, *A&A*, 635, A143, doi: [10.1051/0004-6361/201937233](https://doi.org/10.1051/0004-6361/201937233)
- Gravity Collaboration, Abuter, R., Aymar, N., et al. 2023, *A&A*, 677, L10, doi: [10.1051/0004-6361/202347416](https://doi.org/10.1051/0004-6361/202347416)
- Grishin, E., Bobrick, A., Hirai, R., Mandel, I., & Perets, H. B. 2021, *MNRAS*, 507, 156, doi: [10.1093/mnras/stab1957](https://doi.org/10.1093/mnras/stab1957)
- Guolo, M., Pasham, D. R., Zajaček, M., et al. 2024, *Nature Astronomy*, 8, 347, doi: [10.1038/s41550-023-02178-4](https://doi.org/10.1038/s41550-023-02178-4)
- Hamann, F., & Ferland, G. 1999, *ARA&A*, 37, 487, doi: [10.1146/annurev.astro.37.1.487](https://doi.org/10.1146/annurev.astro.37.1.487)
- Han, W.-B., Yang, S.-C., Tagawa, H., et al. 2024, *arXiv:2401.01743*, doi: [10.48550/arXiv.2401.01743](https://doi.org/10.48550/arXiv.2401.01743)
- Helfand, D. J., White, R. L., & Becker, R. H. 2015, *ApJ*, 801, 26, doi: [10.1088/0004-637X/801/1/26](https://doi.org/10.1088/0004-637X/801/1/26)
- Ho, L. C. 2008, *ARA&A*, 46, 475, doi: [10.1146/annurev.astro.45.051806.110546](https://doi.org/10.1146/annurev.astro.45.051806.110546)
- Hovatta, T., Nieppola, E., Tornikoski, M., et al. 2008, *A&A*, 485, 51, doi: [10.1051/0004-6361/200809806](https://doi.org/10.1051/0004-6361/200809806)
- Hoyle, F., & Lyttleton, R. A. 1939, *Proceedings of the Cambridge Philosophical Society*, 35, 405, doi: [10.1017/S0305004100021150](https://doi.org/10.1017/S0305004100021150)
- Huang, J., Lin, D. N. C., & Shields, G. 2023, *MNRAS*, 525, 5702, doi: [10.1093/mnras/stad2642](https://doi.org/10.1093/mnras/stad2642)
- Inoue, S., & Takahara, F. 1996, *ApJ*, 463, 555, doi: [10.1086/177270](https://doi.org/10.1086/177270)
- Jermyn, A. S., Dittmann, A. J., Cantiello, M., & Perna, R. 2021, *ApJ*, 914, 105, doi: [10.3847/1538-4357/abfb67](https://doi.org/10.3847/1538-4357/abfb67)
- Jermyn, A. S., Dittmann, A. J., McKernan, B., Ford, K. E. S., & Cantiello, M. 2022, *ApJ*, 929, 133, doi: [10.3847/1538-4357/ac5d40](https://doi.org/10.3847/1538-4357/ac5d40)
- Jiang, Y.-F., Stone, J. M., & Davis, S. W. 2014, *ApJ*, 796, 106, doi: [10.1088/0004-637X/796/2/106](https://doi.org/10.1088/0004-637X/796/2/106)
- Kathirgamaraju, A., Li, H., Ryan, B. R., & Tchekhovskoy, A. 2023, *arXiv:2311.03571*, doi: [10.48550/arXiv.2311.03571](https://doi.org/10.48550/arXiv.2311.03571)
- Kato, S., Fukue, J., & Mineshige, S. 2008, *Black-Hole Accretion Disks — Towards a New Paradigm —*
- Khamitov, I. M., Bikmaev, I. F., Gilfanov, M. R., et al. 2023, *arXiv:2309.11308*, doi: [10.48550/arXiv.2309.11308](https://doi.org/10.48550/arXiv.2309.11308)
- Kimura, S. S., Murase, K., & Bartos, I. 2021, *ApJ*, 916, 111, doi: [10.3847/1538-4357/ac0535](https://doi.org/10.3847/1538-4357/ac0535)
- King, A. 2003, *ApJL*, 596, L27, doi: [10.1086/379143](https://doi.org/10.1086/379143)
- Kitaki, T., Mineshige, S., Ohsuga, K., & Kawashima, T. 2021, *PASJ*, 73, 450, doi: [10.1093/pasj/psab011](https://doi.org/10.1093/pasj/psab011)
- Kocsis, B., Yunes, N., & Loeb, A. 2011, *PhRvD*, 84, 024032, doi: [10.1103/PhysRevD.84.024032](https://doi.org/10.1103/PhysRevD.84.024032)
- Lazzati, D., Perna, R., Gompertz, B. P., & Levan, A. J. 2023, *ApJL*, 950, L20, doi: [10.3847/2041-8213/acd18c](https://doi.org/10.3847/2041-8213/acd18c)
- Lazzati, D., Soares, G., & Perna, R. 2022, *ApJL*, 938, L18, doi: [10.3847/2041-8213/ac98ad](https://doi.org/10.3847/2041-8213/ac98ad)
- Lee, A. T., Cunningham, A. J., McKee, C. F., & Klein, R. I. 2014, *ApJ*, 783, 50, doi: [10.1088/0004-637X/783/1/50](https://doi.org/10.1088/0004-637X/783/1/50)
- Levan, A. J., Malesani, D. B., Gompertz, B. P., et al. 2023, *Nature Astronomy*, 7, 976, doi: [10.1038/s41550-023-01998-8](https://doi.org/10.1038/s41550-023-01998-8)
- Li, F.-L., Liu, Y., Fan, X., et al. 2023a, *ApJ*, 950, 161, doi: [10.3847/1538-4357/acd2d1](https://doi.org/10.3847/1538-4357/acd2d1)
- Li, J., Dempsey, A. M., Li, H., Lai, D., & Li, S. 2023b, *ApJL*, 944, L42, doi: [10.3847/2041-8213/acb934](https://doi.org/10.3847/2041-8213/acb934)
- Li, R., & Lai, D. 2022, *MNRAS*, 517, 1602, doi: [10.1093/mnras/stac2577](https://doi.org/10.1093/mnras/stac2577)
- Li, Y.-J., Wang, Y.-Z., Tang, S.-P., & Fan, Y.-Z. 2023c, *arXiv:2303.02973*, doi: [10.48550/arXiv.2303.02973](https://doi.org/10.48550/arXiv.2303.02973)
- Li, Y.-P., Dempsey, A. M., Li, H., Li, S., & Li, J. 2022, *ApJL*, 928, L19, doi: [10.3847/2041-8213/ac60fd](https://doi.org/10.3847/2041-8213/ac60fd)
- Luo, Y., Wu, X.-J., Zhang, S.-R., et al. 2023, *MNRAS*, 524, 6015, doi: [10.1093/mnras/stad2188](https://doi.org/10.1093/mnras/stad2188)
- Mauch, T., Murphy, T., Buttery, H. J., et al. 2003, *MNRAS*, 342, 1117, doi: [10.1046/j.1365-8711.2003.06605.x](https://doi.org/10.1046/j.1365-8711.2003.06605.x)
- McKernan, B., Ford, K. E. S., Cantiello, M., et al. 2022, *MNRAS*, 514, 4102, doi: [10.1093/mnras/stac1310](https://doi.org/10.1093/mnras/stac1310)
- McKernan, B., Ford, K. E. S., Lyra, W., & Perets, H. B. 2012, *MNRAS*, 425, 460, doi: [10.1111/j.1365-2966.2012.21486.x](https://doi.org/10.1111/j.1365-2966.2012.21486.x)
- McKernan, B., Ford, K. E. S., & O’Shaughnessy, R. 2020, *MNRAS*, 498, 4088, doi: [10.1093/mnras/staa2681](https://doi.org/10.1093/mnras/staa2681)
- Milosavljević, M., Couch, S. M., & Bromm, V. 2009, *ApJL*, 696, L146, doi: [10.1088/0004-637X/696/2/L146](https://doi.org/10.1088/0004-637X/696/2/L146)
- Mooley, K. P., Hallinan, G., Bourke, S., et al. 2016, *ApJ*, 818, 105, doi: [10.3847/0004-637X/818/2/105](https://doi.org/10.3847/0004-637X/818/2/105)
- Morton, S. L., Rinaldi, S., Torres-Orjuela, A., et al. 2023, *PhRvD*, 108, 123039, doi: [10.1103/PhysRevD.108.123039](https://doi.org/10.1103/PhysRevD.108.123039)
- Muchotrzeb, B., & Paczynski, B. 1982, *AcA*, 32, 1
- Murphy, T., Kaplan, D. L., Stewart, A. J., et al. 2021, *PASA*, 38, e054, doi: [10.1017/pasa.2021.44](https://doi.org/10.1017/pasa.2021.44)
- Narayan, R., & Yi, I. 1995, *ApJ*, 452, 710, doi: [10.1086/176343](https://doi.org/10.1086/176343)
- Narayan, R., Yi, I., & Mahadevan, R. 1995, *Nature*, 374, 623, doi: [10.1038/374623a0](https://doi.org/10.1038/374623a0)
- Nyland, K., Dong, D. Z., Patil, P., et al. 2020, *ApJ*, 905, 74, doi: [10.3847/1538-4357/abc341](https://doi.org/10.3847/1538-4357/abc341)



- Ofek, E. O., Adams, S. M., Waxman, E., et al. 2021, *ApJ*, 922, 247, doi: [10.3847/1538-4357/ac24fc](https://doi.org/10.3847/1538-4357/ac24fc)
- Ohsuga, K., Mori, M., Nakamoto, T., & Mineshige, S. 2005, *ApJ*, 628, 368, doi: [10.1086/430728](https://doi.org/10.1086/430728)
- Paliya, V. S., Domínguez, A., Ajello, M., Franckowiak, A., & Hartmann, D. 2019, *ApJL*, 882, L3, doi: [10.3847/2041-8213/ab398a](https://doi.org/10.3847/2041-8213/ab398a)
- Palmese, A., Fishbach, M., Burke, C. J., Annis, J., & Liu, X. 2021, *ApJL*, 914, L34, doi: [10.3847/2041-8213/ac0883](https://doi.org/10.3847/2041-8213/ac0883)
- Pan, Z., & Yang, H. 2021, *ApJ*, 923, 173, doi: [10.3847/1538-4357/ac249c](https://doi.org/10.3847/1538-4357/ac249c)
- Park, J., & Tripp, S. 2017, *ApJ*, 834, 157, doi: [10.3847/1538-4357/834/2/157](https://doi.org/10.3847/1538-4357/834/2/157)
- Perna, R., Lazzati, D., & Cantiello, M. 2021a, *ApJL*, 906, L7, doi: [10.3847/2041-8213/abd319](https://doi.org/10.3847/2041-8213/abd319)
- Perna, R., Tagawa, H., Haiman, Z., & Bartos, I. 2021b, *ApJ*, 915, 10, doi: [10.3847/1538-4357/abfdb4](https://doi.org/10.3847/1538-4357/abfdb4)
- Qian, K., Li, J., & Lai, D. 2024, *ApJ*, 962, 143, doi: [10.3847/1538-4357/ad1b53](https://doi.org/10.3847/1538-4357/ad1b53)
- Ray, M., Lazzati, D., & Perna, R. 2023, *MNRAS*, 521, 4233, doi: [10.1093/mnras/stad816](https://doi.org/10.1093/mnras/stad816)
- Rees, M. J., Begelman, M. C., Blandford, R. D., & Phinney, E. S. 1982, *Nature*, 295, 17, doi: [10.1038/295017a0](https://doi.org/10.1038/295017a0)
- Ren, J., Chen, K., Wang, Y., & Dai, Z.-G. 2022, *ApJL*, 940, L44, doi: [10.3847/2041-8213/aca025](https://doi.org/10.3847/2041-8213/aca025)
- Rom, B., Sari, R., & Lai, D. 2024, *ApJ*, 964, 43, doi: [10.3847/1538-4357/ad284b](https://doi.org/10.3847/1538-4357/ad284b)
- Rowan, C., Boekholt, T., Kocsis, B., & Haiman, Z. 2023, *MNRAS*, 524, 2770, doi: [10.1093/mnras/stad1926](https://doi.org/10.1093/mnras/stad1926)
- Samsing, J., Bartos, I., D’Orazio, D. J., et al. 2022, *Nature*, 603, 237, doi: [10.1038/s41586-021-04333-1](https://doi.org/10.1038/s41586-021-04333-1)
- Shakura, N. I., & Sunyaev, R. A. 1973, *A&A*, 24, 337
- Shimwell, T. W., Hardcastle, M. J., Tasse, C., et al. 2022, *A&A*, 659, A1, doi: [10.1051/0004-6361/202142484](https://doi.org/10.1051/0004-6361/202142484)
- Sirko, E., & Goodman, J. 2003, *MNRAS*, 341, 501, doi: [10.1046/j.1365-8711.2003.06431.x](https://doi.org/10.1046/j.1365-8711.2003.06431.x)
- Svensson, R., & Zdziarski, A. A. 1994, *ApJ*, 436, 599, doi: [10.1086/174934](https://doi.org/10.1086/174934)
- Tagawa, H., Haiman, Z., & Kocsis, B. 2020, *ApJ*, 898, 25, doi: [10.3847/1538-4357/ab9b8c](https://doi.org/10.3847/1538-4357/ab9b8c)
- Tagawa, H., Kimura, S. S., Haiman, Z., Perna, R., & Bartos, I. 2023a, *ApJ*, 950, 13, doi: [10.3847/1538-4357/acc4bb](https://doi.org/10.3847/1538-4357/acc4bb)
- , 2023b, *ApJL*, 946, L3, doi: [10.3847/2041-8213/acc103](https://doi.org/10.3847/2041-8213/acc103)
- , 2023c, *arXiv:2310.18392*, doi: [10.48550/arXiv.2310.18392](https://doi.org/10.48550/arXiv.2310.18392)
- Tagawa, H., Kimura, S. S., Haiman, Z., et al. 2022, *ApJ*, 927, 41, doi: [10.3847/1538-4357/ac45f8](https://doi.org/10.3847/1538-4357/ac45f8)
- Takeuchi, S., Mineshige, S., & Ohsuga, K. 2009, *PASJ*, 61, 783, doi: [10.1093/pasj/61.4.783](https://doi.org/10.1093/pasj/61.4.783)
- Tanaka, H., Takeuchi, T., & Ward, W. R. 2002, *ApJ*, 565, 1257, doi: [10.1086/324713](https://doi.org/10.1086/324713)
- Toomre, A. 1964, *ApJ*, 139, 1217, doi: [10.1086/147861](https://doi.org/10.1086/147861)
- Uchiyama, Y., Aharonian, F. A., Tanaka, T., Takahashi, T., & Maeda, Y. 2007, *Nature*, 449, 576, doi: [10.1038/nature06210](https://doi.org/10.1038/nature06210)
- Wandel, A. 1984, *MNRAS*, 207, 861, doi: [10.1093/mnras/207.4.861](https://doi.org/10.1093/mnras/207.4.861)
- Wang, J.-M., Chen, Y.-M., & Hu, C. 2006, *ApJL*, 637, L85, doi: [10.1086/500557](https://doi.org/10.1086/500557)
- Wang, J.-M., Du, P., Baldwin, J. A., et al. 2012, *ApJ*, 746, 137, doi: [10.1088/0004-637X/746/2/137](https://doi.org/10.1088/0004-637X/746/2/137)
- Wang, J.-M., Liu, J.-R., Ho, L. C., & Du, P. 2021a, *ApJL*, 911, L14, doi: [10.3847/2041-8213/abee81](https://doi.org/10.3847/2041-8213/abee81)
- Wang, J.-M., Liu, J.-R., Ho, L. C., Li, Y.-R., & Du, P. 2021b, *ApJL*, 916, L17, doi: [10.3847/2041-8213/ac0b46](https://doi.org/10.3847/2041-8213/ac0b46)
- Wang, J.-M., Liu, J.-R., Li, Y.-R., et al. 2023a, *ApJL*, 958, L40, doi: [10.3847/2041-8213/ad0bd9](https://doi.org/10.3847/2041-8213/ad0bd9)
- Wang, J.-M., Yan, C.-S., Gao, H.-Q., et al. 2010, *ApJL*, 719, L148, doi: [10.1088/2041-8205/719/2/L148](https://doi.org/10.1088/2041-8205/719/2/L148)
- Wang, J.-M., & Zhou, Y.-Y. 1999, *ApJ*, 516, 420, doi: [10.1086/307080](https://doi.org/10.1086/307080)
- Wang, J.-M., Ge, J.-Q., Hu, C., et al. 2011, *ApJ*, 739, 3, doi: [10.1088/0004-637X/739/1/3](https://doi.org/10.1088/0004-637X/739/1/3)
- Wang, J.-M., Zhai, S., Li, Y.-R., et al. 2023b, *ApJ*, 954, 84, doi: [10.3847/1538-4357/acdf48](https://doi.org/10.3847/1538-4357/acdf48)
- Wang, M., Ma, Y., & Wu, Q. 2023c, *MNRAS*, 520, 4502, doi: [10.1093/mnras/stad422](https://doi.org/10.1093/mnras/stad422)
- Wang, Y., Zhu, Z., & Lin, D. N. C. 2024, *MNRAS*, 528, 4958, doi: [10.1093/mnras/stae321](https://doi.org/10.1093/mnras/stae321)
- Wang, Y.-H., Lazzati, D., & Perna, R. 2022, *MNRAS*, 516, 5935, doi: [10.1093/mnras/stac1968](https://doi.org/10.1093/mnras/stac1968)
- Witzel, G., Martinez, G., Willner, S. P., et al. 2021, *ApJ*, 917, 73, doi: [10.3847/1538-4357/ac0891](https://doi.org/10.3847/1538-4357/ac0891)
- Yang, X.-H., Yuan, F., Ohsuga, K., & Bu, D.-F. 2014, *ApJ*, 780, 79, doi: [10.1088/0004-637X/780/1/79](https://doi.org/10.1088/0004-637X/780/1/79)
- Yang, Y., Bartos, I., Fragione, G., et al. 2022, *ApJL*, 933, L28, doi: [10.3847/2041-8213/ac7c0b](https://doi.org/10.3847/2041-8213/ac7c0b)
- Yang, Y., Bartos, I., Gayathri, V., et al. 2019, *PhRvL*, 123, 181101, doi: [10.1103/PhysRevLett.123.181101](https://doi.org/10.1103/PhysRevLett.123.181101)
- Yi, S.-X., & Cheng, K. S. 2019, *ApJL*, 884, L12, doi: [10.3847/2041-8213/ab459a](https://doi.org/10.3847/2041-8213/ab459a)
- Yuan, C., Murase, K., Guetta, D., et al. 2022, *ApJ*, 932, 80, doi: [10.3847/1538-4357/ac6ddf](https://doi.org/10.3847/1538-4357/ac6ddf)
- Zhang, F., Shu, X., Sun, L., et al. 2022, *ApJ*, 938, 43, doi: [10.3847/1538-4357/ac8a9a](https://doi.org/10.3847/1538-4357/ac8a9a)
- Zhang, S.-R., Luo, Y., Wu, X.-J., et al. 2023, *MNRAS*, 524, 940, doi: [10.1093/mnras/stad1855](https://doi.org/10.1093/mnras/stad1855)
- Zhu, J.-P., Zhang, B., Yu, Y.-W., & Gao, H. 2021a, *ApJL*, 906, L11, doi: [10.3847/2041-8213/abd412](https://doi.org/10.3847/2041-8213/abd412)
- Zhu, J.-P., Wu, S., Yang, Y.-P., et al. 2021b, *ApJ*, 917, 24, doi: [10.3847/1538-4357/abfe5e](https://doi.org/10.3847/1538-4357/abfe5e)